6
One-Dimensional Zonal Model

Some of the reported parametric and modeling studies for an open volumetric air receivers and are reviewed in Chapter 2. In particular, Hoffschmidt *et al*. (2003) experimentally demonstrated that the temperature difference within and among the different absorbers even exceed 100 ˚C with reference to the highest value of about 700 – 800 ˚C. This may lead to failure of such a receiver at a high level of heat flux. Further, the reported wide variation in the receiver thermal efficiencies may be attributed to the cumulative effect of thermal non-uniformity and the heat losses. Thus, a o*ne-dimensional zonal model* is developed in which the absorbers are classified as central or peripheral basing on their relative position and the concentrated heat flux. The model also includes the heat transfer by return air around these absorbers and is the next logical step to an over-simplified one-dimensional model. The detailed development is presented subsequently.

6.1 MATHEMATICAL MODELING

In the designed open volumetric air receiver seven absorbers are enclosed within a casing, as shown in Figure 6.1. Out of which the six peripheral absorbers (P) surround the central counter-part (C). The return air is circulated around the absorbers to limit their temperature and to achieve the peripheral thermal uniformity as far as possible. The direction of primary and return airflow is opposite in nature. The absorbers are externally cooled and the temperature redistribution is a consequence of the return air that leaves the receiver and mixes with the ambient air. A part of the mixed air returns through the absorber pores as the primary air. The fraction of return air ($\dot{m}_r$) that enters the absorbers is called the air return ratio (ARR) and is given by,

$$\frac{\dot{m}_r}{\dot{m}_{total}} = ARR \ . \tag{6.1}$$

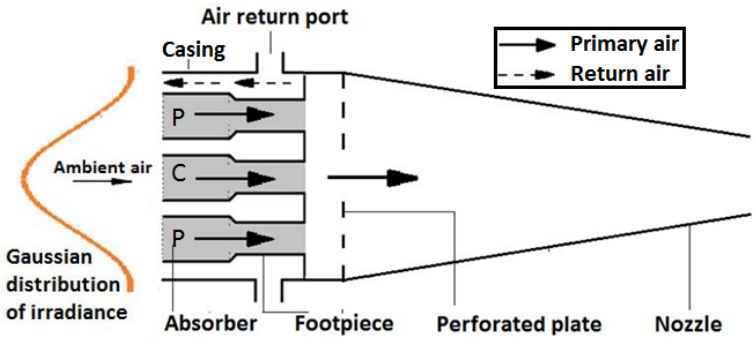

Figure 6.1: Working of open volumetric air receiver (P: Peripheral absorber, C: Central absorber).

The performance or thermal efficiency of an open volumetric air receiver may depend on operating conditions, ARR, absorber porosity and other dimensionless parameters, like gap to diameter ratio, absorber length to diameter ratio. The one-dimensional zonal model may be beneficial for identifying the important parameters lends to an optimal receiver design and its scale-up. The model development is based upon the reported quasi-Gaussian heat flux

distribution on the receiver aperture. Thus, the central absorbers (C) will be exposed to a higher heat flux than that of the peripheral absorbers (P) (see Figure 6.1). Geometrically, the peripheral absorbers are in a close proximity to the receiver enclosure. Whereas, the central absorber is surrounded by the six peripheral absorbers in the current design. A radiative heat exchange is considered between the central and peripheral absorbers. All the peripheral absorbers are assumed to be at the same temperature, hence the radiative heat exchange is neglected between the peripheral counterparts. All these aspects are considered for developing the zonal model. Thus, the outcome is expected to be more realistic than that of an over-simplified one-dimensional single-zone model. The front-view of the receiver as in Figure 6.2(a) shows that the 60° section is based on the symmetry (see Figure 6.2(b)). This consists of one peripheral and 1/6th of the central absorber with the casing.

The return air flow regions around these absorbers are indicated by r_p and r_c,. The return air flow around the absorbers is three-dimensional in nature and the presence of vortex around the central absorber is shown by Sharma *et al*. (2015a,b). This mitigates the thermal non-uniformity, which is beneficial for the receiver integrity. Reproducing the true effect of such a flow feature using a one-dimensional approach is not possible. However, this may be partly introduced by adopting the heat transfer coefficient from the flow around a tube-bundle. The turbulent flow around an absorber is desired for promoting the thermal uniformity. However, the laminar flow is expected in the smallest gap between absorbers or around the central absorber owing to the viscous effect. Assuming the Prandtl number of air as unity, for the thermally fully developed flow, the boundary layer thickness will extend up-to the half of smallest gap (G), see Figure 6.3(a). The heat transfer coefficient for the laminar flow is lower than that of the turbulent flow. This worst-case scenario is employed for identifying the region of influence around the central absorber (r_c) as in Figure 6.3(a). The rest of the return air region is distributed around the peripheral absorber (r_p), which is non-uniform. Indeed, the mass flow rates of return air through these regions will be different as a consequence of flow resistance. A higher return air flow rate is expected around the peripheral absorber compare to the central one. However, the mass flux must be identical for the continuity and is as follows:

$$\frac{\dot{m}_{return}}{A_{return}} = \frac{\dot{m}_{rc}}{A_{rc}} = \frac{\dot{m}_{rp}}{A_{rp}} \tag{6.2}$$

here, $A_{return} = \pi[r_{cas\_i}^2 - 7r_{ab}^2]$, $A_{rc} = \frac{\pi}{6}\mathrm{G}[2r_{ab} + G]$ and $A_{rp} = \frac{A_{return}}{6} - A_{rc}$

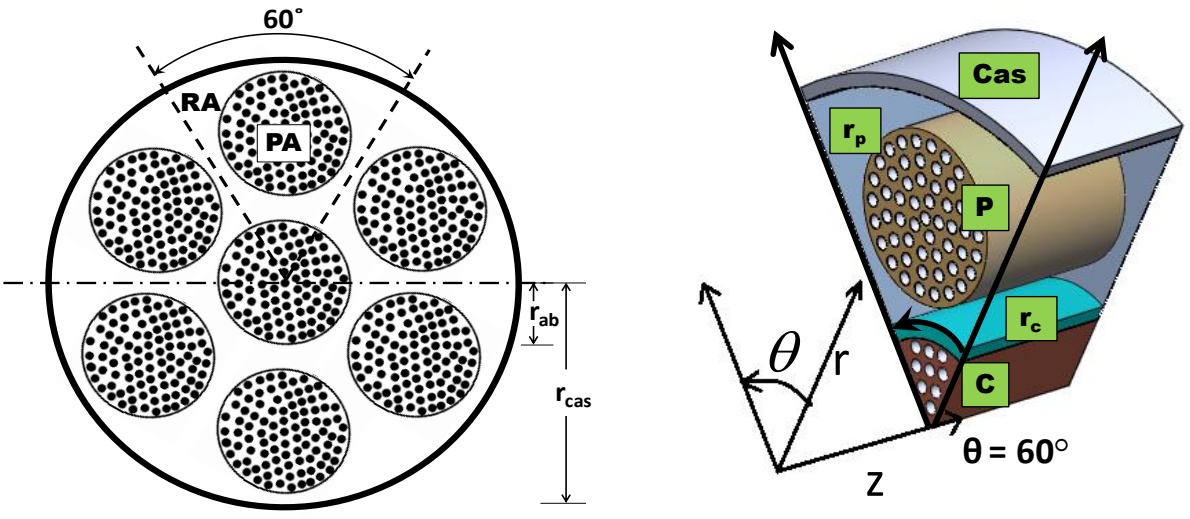

(a) Front view of OVAR

(b) 1/6th section of absorber with casing

Figure 6.2: Front (a) and part view (b) of the OVAR. RA: return air; PA: primary air; C &P: central and peripheral absorber; r_c and r_p: return air regions around C and P, respectively.

To deduce the governing equations for one-dimensional zonal model the area of influence around C and P is redistributed as explained. Due care is taken to preserve both A_{rc} and A_{rp} as in eq. (6.2). This results in the annular flow regions around C and P as shown in Figure 6.3(b) and (c). Also, the surface area of casing is maintained by using a suitable perimeter around P as shown in Figure 6.3(b) using the symbol *cas*. Moreover, a section of receiver with the selected differential element for analysis is depicted in Figure 6.3(d). The required ingredients for the zonal model are discussed subsequently that are essential in the derivation.

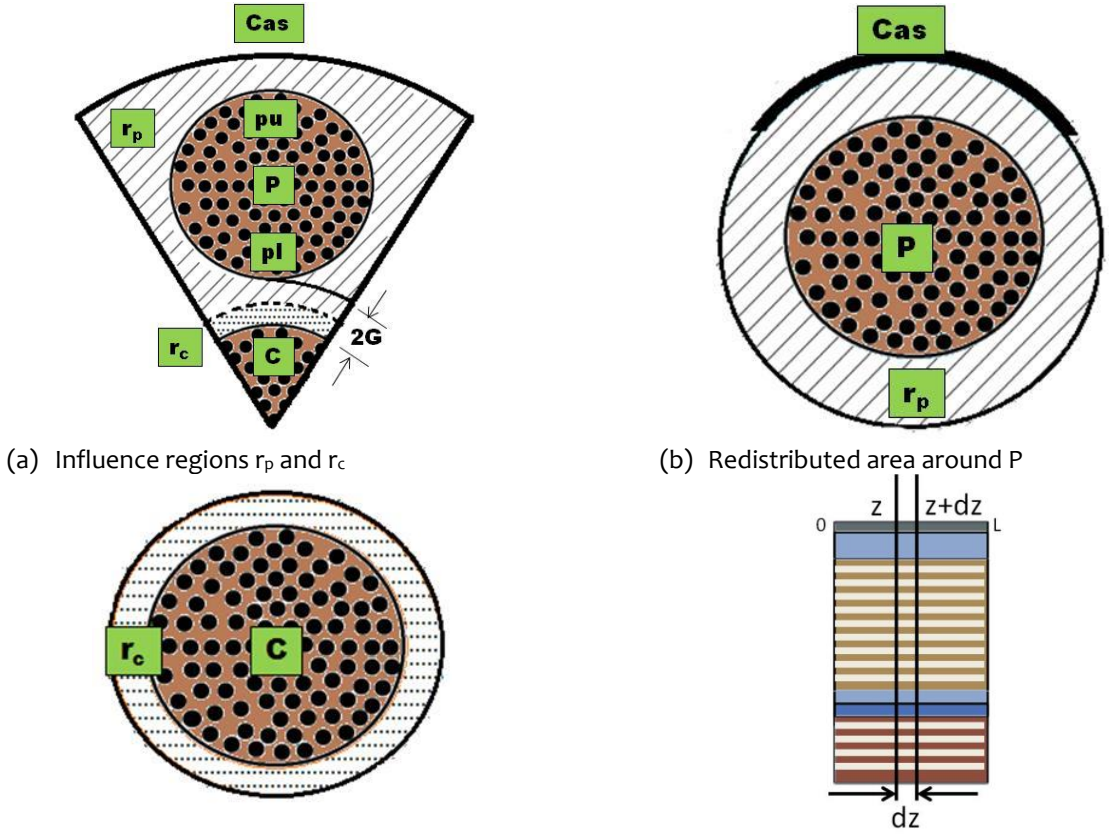

(a) Influence regions r_p and r_c (b) Redistributed area around P

(c) Redistributed area around C (d) Differential element (dz)

Figure 6.3: Influence regions and their redistributions (a, b, c); a differential element along the axial-direction (z) for analysis (d).

6.1.1 Material Properties

In this analysis air is treated as an ideal gas and its thermo-physical properties, viz. specific heat and thermal conductivity are represented as in eq. (6.3) for a temperature range of 300 K to 2000 K [Philip, 2002]. Brass is used as absorber material with constant properties viz. specific heat (c_p= 380 kJ/kgK), thermal conductivity (k = 111 W/mK) and density (ρ = 8600 kg/m^3).

$$\left.\begin{aligned} c_{p\_air} &= T_{air}^4 \times 10^{-10} - T_{air}^3 \times 5\times 10^{-7} + T_{air}^2 \times 8\times 10^{-4} - 0.3T_{air} + 1032.1 \\ k_{air} &= T_{air}^3 \times 7\times 10^{-12} - T_{air}^2 \times 3\times 10^{-8} + T_{air} \times 9\times 10^{-5} + 0.0008 \end{aligned}\right\} \quad (6.3)$$

6.1.2 Heat Transfer Correlations: Nusselt Number

A heat transfer correlation is needed for the forced convection in and around absorber involving the primary and the return air. Generally, the flow inside an absorber pore is laminar with Re_D ~200. For the fully developed laminar flow Nusselt number (Nu) is 4.36 at a constant

heat flux. However, an insufficient absorber length necessitates the need of dedicated *Nu* correlation, which is adopted from Subbarao (2015) and is given in eq. (6.4).

$$Nu = 4.36 + \frac{0.086(\mathrm{Re}_D \mathrm{Pr}\frac{d}{L})^{1.33}}{1 + 0.1\mathrm{Pr}(\mathrm{Re}_D \frac{d}{L})^{0.83}} \tag{6.4}$$

The return air side is treated as annular in the zonal model. However, to reflect the effect of flow three-dimensionality on the heat transfer the tube-bundle correlations are adopted from literature including the one, which is based on a computational analysis by Sarma (2013). These are listed in Table 6.1. The required view factor in the zonal model is discussed subsequently.

Table 6.1: Correlations for Nusselt number used in return air side.

Correlation	Geometry	Formulation
Kays *et al*., (1972)	Annular region	From data table
Žukauskas, (1972)	Tube bundle	$Nu = C\,\mathrm{Re}^m\,\mathrm{Pr}^n\left(\frac{\mathrm{Pr}}{\mathrm{Pr}_s}\right)^{1/4}$; $0.7 \le \mathrm{Pr} \le 500; 1 \le \mathrm{Re} \le 10^6$
Grimison, (1937)	Tube bundle	$Nu = 0.44\,\mathrm{Re}_{max}^{0.556}\,\mathrm{Pr}^{1/3}$ (Using coefficients table)
Sarma, (2013)	Open volumetric air receiver	$Nu = 0.345\,\mathrm{Re}^{0.597}$

6.1.3 Calculation of View Factors

6.1.3.1 View Factor between Central and Peripheral Absorber

The view factor between two infinitely long bodies of given cross-sections is calculated using the Hottel's cross string method. Following relation is used considering two bodies (1&2):

$$L_1F_{12} = L_2F_{21} = \frac{\text{Total crossed strings (CS) length} - \text{Total uncrossed strings (US) length}}{2} \tag{6.5}$$

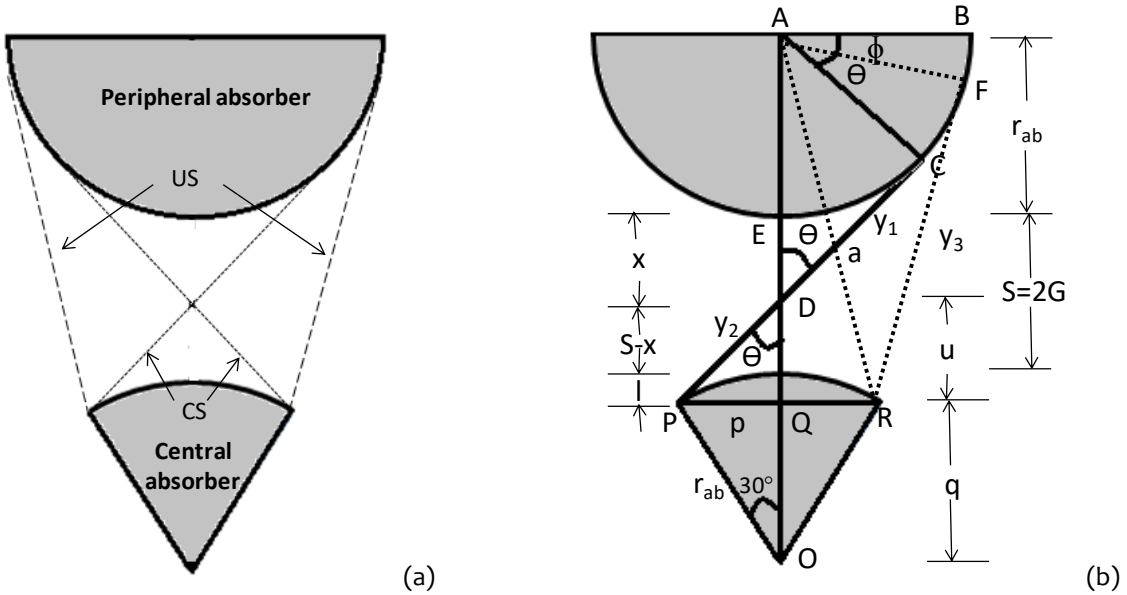

(a) (b)

Figure 6.4: A schematic showing (a) Crossed (CS) and un-crossed (US) strings and (b) dimensional quantities for view factor calculation between peripheral and central absorbers.

where, L_1 and L_2 are the string lengths on the bodies 1 and 2 respectively. On a convex body, length of the string will be a part of its perimeter. In Figure 6.4(a), the crossed strings (CS) and uncrossed strings (US) of equal length are shown. Assuming infinitely long bodies, the end losses are neglected for the view factor calculation. The considered 180° section of the peripheral absorber (P) and 60° section of the central absorber (C) are shown in Figure 6.4(b). The absorbers are separated by a distance S (=2G). A tangent is drawn on the peripheral absorber from a point P on central absorber, which intersects the line joining the centers of absorbers at D. The distance of point D from the point E is x. The calculations for the crossed string length (PB) are:

From ΔPOQ,

$$\begin{aligned} p &= r_{ab}\sin 30^\circ = r_{ab}/2, \\ q &= r_{ab}\cos 30^\circ = \left(\sqrt{3}/2\right) r_{ab}, \\ u &= S - x + l, \\ l &= r_{ab} - q = \left(1 - \sqrt{3}/2\right) r_{ab}, \\ \Rightarrow u &= S - x + \left(1 - \sqrt{3}/2\right) r_{ab}. \end{aligned} \tag{6.6}$$

From ΔADC and ΔPDQ,

$$\tan\theta = \frac{r}{y_1} = \frac{p}{u},$$

$$\Rightarrow y_1 = 2u. \tag{6.7}$$

Also,

$$\sin\theta = \frac{r_{ab}}{r_{ab} + x} = \frac{p}{y_2},$$

$$\Rightarrow y_2 = \frac{r_{ab} + x}{2}. \tag{6.8}$$

Using Pythagoras theorem in ΔPDQ gives

$$y_2^2 = u^2 + p^2. \tag{6.9}$$

Solving for x using eq. (6.6) and eq. (6.8),

$$x = (0.512 r_{ab} + 1.33S) - \sqrt{0.44S^2 + 0.2382 r_{ab}^2 + 1.008 r_{ab} S}. \tag{6.10}$$

The values for y_1 and y_2 and $arcBC$ can be calculated using x. Now for the uncrossed string (RB), a tangent is drawn from the point R to F. The length y_3 of the tangent is calculated using Pythagoras theorem as follows:

In ΔARQ and ΔAFR,

$$a^2 = (r_{ab} + S + l)^2 + p^2,$$

and,

$$a^2 = {r_{ab}}^2 + y_3^2,$$

$$\Rightarrow y_3 = \sqrt{0.536 r_{ab}^2 + S^2 + 2.268 S r_{ab}}. \tag{6.11}$$

From the crossed string method,

$$L_c F_{c-pl} = L_{pl} F_{pl-c} = \frac{\text{total } \textit{Crossed} \text{ string length} - \text{total } \textit{Uncrossed} \text{ string length}}{2},$$

$$\Rightarrow L_c F_{c-pl} = L_{pl} F_{pl-c} = \frac{2(y_1 + y_2 + arcBC) - 2(y_3 + arcBF)}{2},$$

$$\Rightarrow L_c F_{c-pl} = L_{pl} F_{pl-c} = \left(y_1 + y_2 + 2\pi r_{ab} \frac{\tan^{-1}(r_{ab}/y_1)}{360} \right) - \left(y_3 + 2\pi r_{ab} \frac{\tan^{-1}(r_{ab}/y_3)}{360} \right). \quad (6.12)$$

Where, L_c and L_{pl} are the perimeters of sections of central and peripheral absorbers respectively. Using this method, the calculated view factor between two semi-cylinders of equal radii with their convex sides facing each other is 0.287, which is comparable to Incropera *et al*. (2012) that confirms the derived parameters. For the current open volumetric air receiver design with the seven absorbers (see Figure 6.1), the view factors from C to P is $F_{c\text{-}pl}$= *0.30* and from P to C is $F_{pl\text{-}c}$= *0.10*. These parameters are employed for analyzing heat transfer in peripheral and central absorbers.

6.1.3.2 Calculation of View Factor between Casing and Peripheral Absorber

The inner side of casing exchanges heat with the peripheral absorber via radiation. The calculation for view factor is based on the laws of radiative heat exchange that are summation and reciprocity rules. Here, the geometry is divided into four regions as shown in Figure 6.5(a). The region 1 is on the peripheral absorber and region 3 is on the casing. The tangents *C'B* and *GH* are named as regions 2 and 4, respectively. The summation rule for the given regions is as follows:

$$\sum_{j=1}^{n} F_{ij} = 1$$

$$\Rightarrow \left.\begin{aligned} F_{11} + F_{12} + F_{13} + F_{14} &= 1 \\ F_{21} + F_{22} + F_{23} + F_{24} &= 1 \\ F_{31} + F_{32} + F_{33} + F_{34} &= 1 \\ F_{41} + F_{42} + F_{43} + F_{44} &= 1 \end{aligned}\right\} \quad (6.13)$$

The following assumptions are used in the calculations:

1. F_{ii} = 0 i.e. the view factor of all the regions with themselves is zero.
2. On the basis of symmetry of the geometry, the following view factors are equal $F_{23} = F_{43}$, $F_{32} = F_{34}$, $F_{21} = F_{41}$, $F_{12} = F_{14}$ and $F_{24} = F_{42}$.

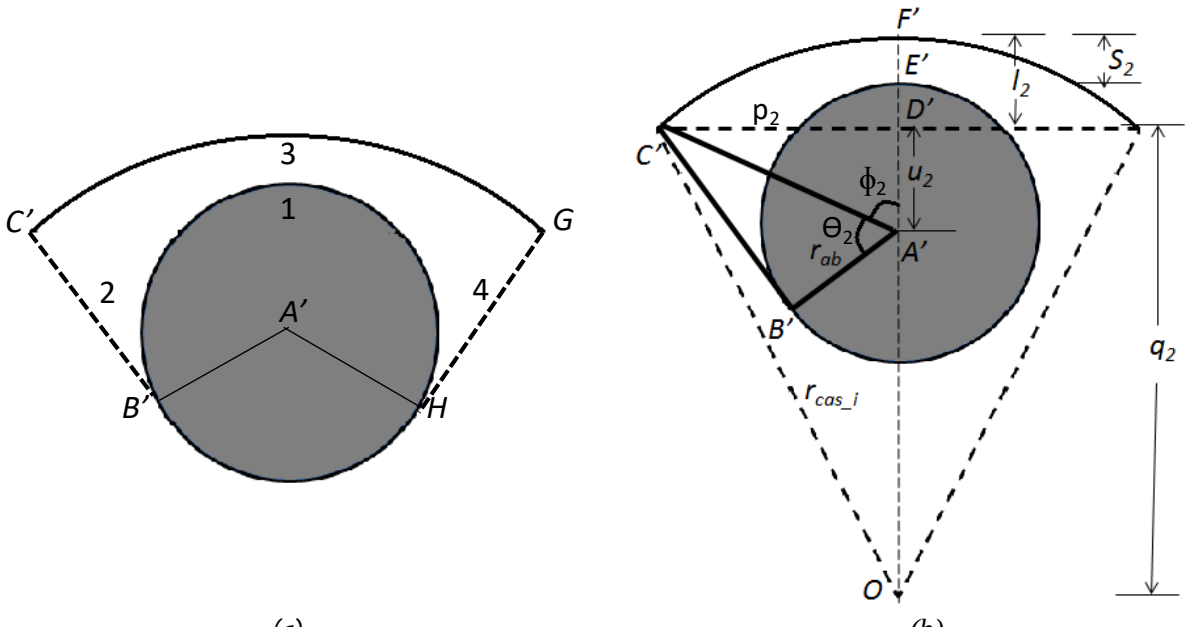

(a) *(b)*

Figure 6.5: Schematics of (a) Regions for shape factor calculation, (b) calculation of length of regions.

Using the assumptions, the set of equations becomes:

$$\left.\begin{aligned} 2F_{12}+F_{13}&=1\\ F_{21}+F_{23}&=1\\ F_{31}+2F_{32}&=1 \end{aligned}\right\} \tag{6.14}$$

Using reciprocity,

$$F_{21}=\frac{A_1}{A_2}F_{12},\ F_{31}=\frac{A_1}{A_3}F_{13},\ F_{32}=\frac{A_2}{A_3}F_{23}\ , \tag{6.15}$$

$$\left.\begin{aligned} &2F_{12}+F_{13}=1\\ \Rightarrow\ &\frac{A_1}{A_2}F_{12}+F_{23}=1\\ &\frac{A_1}{A_3}F_{13}+2\frac{A_2}{A_3}F_{23}=1 \end{aligned}\right\}, \tag{6.16}$$

$$\Rightarrow F_{13}=\frac{A_1-2A_2+A_3}{2A_1}\ \text{and}\ F_{31}=\frac{A_1-2A_2+A_3}{2A_3}\ .$$

For a fixed width we get,

$$F_{13}=\frac{L_1-2L_2+L_3}{2L_1}\ \text{and}\ F_{31}=\frac{L_1-2L_2+L_3}{2L_3}\ .$$

Following the adopted nomenclature of the model, the view factors can be written as:

$$F_{pu-cas}=\frac{L_{pu}-2L_2+L_{cas}}{2L_{pu}}\ \text{and}\ F_{cas-pu}=\frac{L_{pu}-2L_2+L_{cas}}{2L_{cas}} \tag{6.17}$$

Using Figure 6.5(b), the lengths of the regions 1-4 are calculated as following:

In $\Delta OC'D'$,

$$\begin{aligned} p_2&=r_{cas\_i}\sin 30^\circ=r_{cas\_i}/2,\\ q_2&=r_{cas\_i}\cos 30^\circ=\left(\sqrt{3}/2\right)r_{cas\_i},\\ u_2&=r_{ab}+s_2-l_2,\\ l_2&=r_{cas\_i}-q_2=\left(1-\frac{\sqrt{3}}{2}\right)r_{cas\_i},\\ \Rightarrow u_2&=r_{ab}+s_2-\left(1-\frac{\sqrt{3}}{2}\right)r_{cas\_i}. \end{aligned} \tag{6.18}$$

In $\Delta C'A'B'$ and $\Delta C'A'D'$, using the Pythagoras theorem gives,

$$\begin{aligned} &L_2^2+r_{ab}^2=b^2=p_2^2+u_2^2\\ &\Rightarrow L_2=\sqrt{\frac{r_{cas\_i}^2}{4}+u_2^2-r_{ab}^2} \end{aligned} \tag{6.19}$$

and,

$$L_{pu} = 2.arcB'E' ,$$

$$\Rightarrow L_{pu} = 4\pi r_{ab}\left(\frac{\tan^{-1}(L_2 / r_{ab}) + \tan^{-1}(r_{cas\_i} / 2u_2)}{360}\right). \quad (6.20)$$

Finally, the length of region 3 is given by,

$$L_{cas} = \frac{\pi r_{cas\_i}}{3} . \quad (6.21)$$

In the present case, the shape factors are $F_{pu\text{-}cas}$ and $F_{cas\text{-}pu}$ are 0.53 and 0.59 respectively. The derived relations for the view factors are applied in the energy equations for the casing and the peripheral absorber. These are presented subsequently.

6.2 THE GOVERNING EQUATIONS

6.2.1 Casing

The heat exchange between casing with peripheral absorbers and the return air is illustrated in Figure 6.6. For brevity and generality, it is assumed that the casing will be exposed to the same concentrated irradiance on-the-field as the peripheral absorber. The instantaneous conservation of energy in the differential element dz results in:

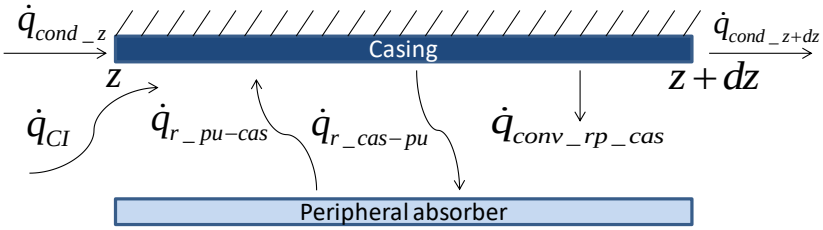

Figure 6.6: Energy balance for casing.

Rate of energy input ($\dot{q}_{in}$) = Rate of energy incident from heliostats ($\dot{q}_{CI}$) via radiation + Rate of conductive heat transfer at z ($\dot{q}_{cond\_z}$) + Rate of radiative heat transfer from peripheral absorber ($\dot{q}_{r\_pu-cas}$)

Rate of energy out ($\dot{q}_{out}$) = Rate of convective heat transfer to return air ($\dot{q}_{conv\_rp\_cas}$) + Rate of conductive heat transfer at $z+dz$ ($\dot{q}_{cond\_z+dz}$) + Rate of radiative heat transfer to peripheral absorber ($\dot{q}_{r\_cas-pu}$)

Rate of internal heat generation ($\dot{q}_{gen}$) = 0

Rate of energy stored ($\dot{q}_{st}$) = $dm_{cas}c_{p\_cas}\frac{\partial T_{cas}}{\partial t}$

$$\therefore \dot{q}_{in} - \dot{q}_{out} + \dot{q}_{gen} = \dot{q}_{st}$$

$$\Rightarrow \dot{q}_{CI} + \dot{q}_{cond\_z} + \dot{q}_{r\_pu-cas} - (\dot{q}_{conv\_rp\_c} + \dot{q}_{cond\_z+dz} + \dot{q}_{r\_cas-pu}) = \dot{q}_{st}$$

$$\left.\begin{aligned} &\underbrace{k_{cas}A_{cas\_c}\frac{\partial^2 T_{cas}}{\partial z^2}.\mathrm{dz}}_{\textit{Conduction}\text{ term}} + \underbrace{q''_{in-cas}dA_{cas\_s}}_{\textit{Radiation}\text{ term}} + \underbrace{\frac{\sigma(T_p^4 - T_{cas}^4)}{\left(\frac{1-\in_{ab}}{\in_{ab}\,dA_{pu}}\right)+\frac{1}{dA_{pu}F_{pu-cs}}+\left(\frac{1-\in_{cas}}{\in_{cas}\,dA_{cas\_s}}\right)}}_{\textit{Radiation}\text{ heat exchange term}} \\ \Rightarrow\quad & \\ &-\underbrace{h_{rp\_cas}dA_{cas\_s}(\mathrm{T}_{cas}-T_{rp})}_{\textit{Convection}\text{ term}} = \underbrace{dm_{cas}c_{p\_cas}\frac{\partial T_{cas}}{\partial t}}_{\textit{Storage}\text{ term}} \end{aligned}\right\} \tag{6.22}$$

Assuming an enclosure and from the principle of reciprocity:

$$dA_{pu}F_{pu-cas} = dA_{cas}F_{cas-pu}$$

$$\left.\begin{aligned} &\underbrace{\left(\frac{k_{cas}}{\rho_{cas}c_{p\_cas}}\right)\frac{\partial^2 T_{cas}}{\partial \mathrm{z}^2}}_{\textit{Conduction}\text{ term}} + \underbrace{\left(\frac{2r_{cas\_i}}{\rho_{cas}c_{p\_cas}(r_{cas\_o}^2 - r_{cas\_\mathrm{i}}^2)}\right)q''_{in-cas}}_{\textit{Radiation}\text{ term}} - \underbrace{\left(\frac{2h_{rp\_cas}r_{cas\_\mathrm{i}}}{\rho_{cas}c_{p\_cas}(r_{cas\_o}^2 - r_{cas\_\mathrm{i}}^2)}\right)(\mathrm{T}_{cas}-T_{rp})}_{\textit{Convection}\text{ term}} \\ \Rightarrow\quad & \\ &\underbrace{+\frac{\sigma(T_p^4 - T_{cas}^4)}{\rho_{ab}c_{p\_\mathrm{p}}\left[\left(\frac{1-\in_{ab}}{\in_{ab}}\right)\left(\frac{(1-\varepsilon)\pi r_{ab}^2}{L_{pu}}\right)+\frac{(1-\varepsilon)\pi r_{ab}^2}{L_{pu}F_{pu-cas}}+\left(\frac{1-\in_{cas}}{\in_{cas}}\right)\left(\frac{3(1-\varepsilon)r_{ab}^2}{r_{cas\_i}}\right)\right]}}_{\text{Net }\textit{radiative}\text{ heat transfer at casing}} = \underbrace{\frac{\partial T_{cas}}{\partial t}}_{\textit{Transient}\text{ term}} \end{aligned}\right\} \tag{6.23}$$

$$\Rightarrow\ u_1\frac{\partial^2 T_{cas}}{\partial \mathrm{z}^2} + v_1 q''_{in-cas} - w_1(\mathrm{T}_{cas}-T_{rp}) + x_1(T_p^4 - T_{cas}^4) = \frac{\partial T_{cas}}{\partial t} \tag{6.24}$$

Initial condition:
At $t = 0,\ T_{cas} = T_{atm}$.

Boundary conditions:
The net heat transfer due to incident and loss by radiation at the inlet is as follows:
At $z = 0,\ -k_{cas}\frac{\partial T_{cas}}{\partial \mathrm{z}} = q''_{in\_cas} - \sigma \in_{cas} (T_{cas}^4 - T_{atm}^4)$.

Adiabatic boundary condition at the outlet ($z = L$), $\frac{\partial T_{cas}}{\partial \mathrm{z}} = 0$.

where,

$A_{cas\_c} = \pi(r_{cas\_o}^2 - r_{cas\_\mathrm{i}}^2)\times 1/6,$

$dA_{cas\_s} = 2\pi r_{cas\_i}.dz \times 1/6,$

$dm_{cas} = \rho_{cas} d\forall_{cas},$

$q''_{in\_cas} = (POA)_{cas} / A_{cas\_c},$

$d\forall_{cas} = \frac{1}{6}\pi(\mathrm{r}_{cas\_o}^2 - \mathrm{r}_{cas\_i}^2)dz,$

$u_1 = \left(\frac{k_{cas}}{\rho_{cas}c_{p\_cas}}\right),$

$$v_1 = \left(\frac{2r_{cas\_i}}{\rho_{cas} c_{p\_cas} (r_{cas\_o}^2 - r_{cas\_i}^2)} \right),$$

$$w_1 = \left(\frac{2h_{rp\_cas} r_{cas\_i}}{\rho_{cas} c_{p\_cas} (r_{cas\_o}^2 - r_{cas\_i}^2)} \right),$$

$$x_1 = \frac{\sigma}{\rho_{ab} c_{p\_p} \left[\left(\frac{1-\epsilon_{ab}}{\epsilon_{ab}} \right) \left(\frac{(1-\varepsilon)\pi r_{ab}^2}{L_{pu}} \right) + \frac{(1-\varepsilon)\pi r_{ab}^2}{L_{pu} F_{pu-cas}} + \left(\frac{1-\epsilon_{cas}}{\epsilon_{cas}} \right) \left(\frac{3(1-\varepsilon) r_{ab}^2}{r_{cas\_i}} \right) \right]}.$$

6.2.2 Absorbers

6.2.2.1 Peripheral Absorber

Peripheral absorbers have a radiative heat exchange with casing, a radiative heat exchange with central absorber, and convective heat exchange with primary and return air as in Figure 6.7.

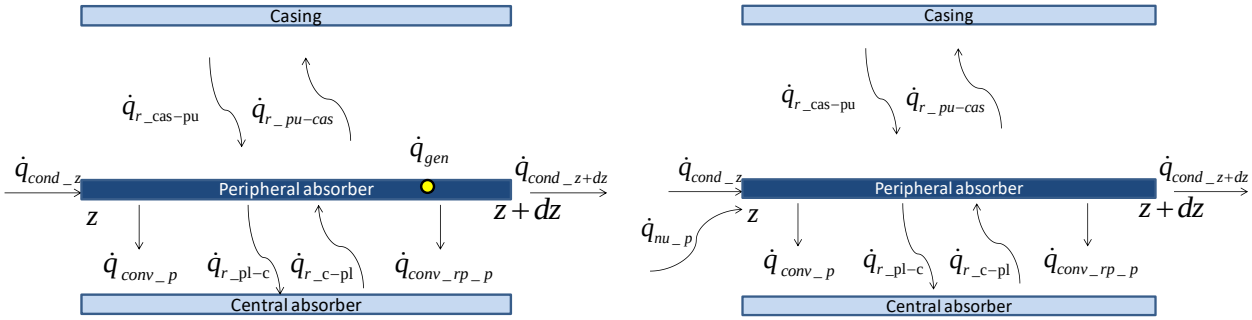

(a) Volumetric heat generation (b) Non-uniform heat flux

Figure 6.7: Energy balance for peripheral absorber.

Rate of energy in ($\dot{q}_{in}$) = Rate of conductive heat transfer at z ($\dot{q}_{cond\_z}$) + Rate of radiative heat transfer from casing to the upper part of peripheral absorber ($\dot{q}_{r\_cas-pu}$) + Rate of radiative heat transfer from central absorber to the lower part of peripheral absorber ($\dot{q}_{r\_c-pl}$) + Rate of incident concentrated irradiance from heliostats ($\dot{q}_{nu\_p}$)

Rate of energy out ($\dot{q}_{out}$) =
Rate of convective heat transfer to primary air ($\dot{q}_{conv\_a\_p}$) + Rate of convective heat transfer to return air ($\dot{q}_{conv\_rp\_p}$) + Rate of conductive heat transfer at z+dz ($\dot{q}_{cond\_z+dz}$) + Rate of radiative heat transfer from casing ($\dot{q}_{r\_pu-cas}$) + Rate of radiative heat transfer from central absorber ($\dot{q}_{r\_pl-c}$)

Rate of heat generation in case of volumetric heating ($\dot{q}_{gen}$) = $\dot{q}_{gen\_p} d\forall_{ab\_p}$

Rate of energy stored ($\dot{q}_{st}$) = $\rho_{ab} d\forall_{ab\_p} c_{p\_p} \frac{\partial T_p}{\partial t}$

Energy balance gives

$$\dot{q}_{in} - \dot{q}_{out} + \dot{q}_{gen} = \dot{q}_{st}$$

$$\left.\begin{aligned}
&\underbrace{k_p A_{p_c}\frac{\partial^2 T_p}{\partial z^2}\mathrm{dz}}_{\text{Conduction term}}+\underbrace{\frac{\sigma(T_{cas}^4-T_p^4)}{\left(\frac{1-\in_{cas}}{\in_{cas}\,dA_{cas_s}}\right)+\frac{1}{dA_{cas_s}F_{cas_pu}}+\left(\frac{1-\in_{ab}}{\in_{ab}\,dA_{pu}}\right)}}_{\text{Radiation heat exchange with casing}}+\underbrace{\frac{\sigma(T_c^4-T_p^4)}{\left(\frac{1-\in_{ab}}{\in_{ab}\,dA_{c_s}}\right)+\frac{1}{dA_{c_s}F_{c_pl}}+\left(\frac{1-\in_{ab}}{\in_{ab}\,dA_{pl}}\right)}}_{\text{Radiation heat exchange with central absorber}}\\
&\Rightarrow\underbrace{-h_{a_p}dA_{\mathrm{nh_p}}(\mathrm{T}_p-T_{a_p})}_{\text{Convective loss to primary air}}\underbrace{-h_{rp_\mathrm{p}}dA_{\mathrm{p_s}}(\mathrm{T}_p-T_{rp})}_{\text{Convective loss to return air}}+\underbrace{\dot{q}_{s_p}}_{\text{Source term}}=\underbrace{\rho_{ab}d\forall_{ab_p}c_{p_\mathrm{p}}\frac{\partial T_p}{\partial t}}_{\text{Storage term}}\\
&\text{here, }\dot{q}_{s_\mathrm{p}}=\begin{cases}\underbrace{\dot{q}_{gen_p}d\forall_{ab_p}}_{\text{Volumetric heat generation}}\\ \underbrace{q''_{nu_p}dA_{nh_p}}_{\text{Non-uniform heat flux}}\end{cases}
\end{aligned}\right\}\quad(6.25)$$

After simplification of terms, the equation becomes:

$$\left.\begin{aligned}
&\underbrace{\left(\frac{k_p}{\rho_p c_{p_\mathrm{p}}}\right)\frac{\partial^2 T_p}{\partial z^2}}_{\text{Conduction term}}+\underbrace{\frac{\sigma(T_{cas}^4-T_p^4)}{\rho_{ab}c_{p_\mathrm{p}}\left[\left(\frac{1-\in_{ab}}{\in_{ab}}\right)\left(\frac{(1-\varepsilon)\pi r_{ab}^2}{L_{pu}}\right)+\frac{(1-\varepsilon)\pi r_{ab}^2}{L_{pu}F_{pu-cas}}+\left(\frac{1-\in_{cas}}{\in_{cas}}\right)\left(\frac{3(1-\varepsilon)r_{ab}^2}{r_{cas_i}}\right)\right]}}_{\text{Net radiatve heat exchange with casing}}\\
&\Rightarrow+\underbrace{\frac{\sigma(T_c^4-T_p^4)}{\rho_{ab}c_{p_\mathrm{p}}\left[\left(\frac{1-\in_{ab}}{\in_{ab}}\right)\left((1-\varepsilon)3\pi r_{ab}\right)+\frac{(1-\varepsilon)3\pi r_{ab}}{F_{c-pl}}+\left(\frac{1-\in_{ab}}{\in_{ab}}\right)(1-\varepsilon)r_{ab}\right]}}_{\text{Net radiative heat exchange with central absorber}}\\
&\underbrace{-\left(\frac{2nh_{a_p}r_h}{\rho_p c_{p_\mathrm{p}}(1-\varepsilon).r_{ab}^{\,2}}\right)(\mathrm{T}_p-T_{a_p})}_{\text{Convective loss to primary air}}\underbrace{-\left(\frac{2h_{rp_\mathrm{p}}}{\rho_p c_{p_\mathrm{p}}(1-\varepsilon).r_{ab}}\right)(\mathrm{T}_p-T_{rp})}_{\text{Convective loss to return air}}+\underbrace{\left(\frac{\dot{q}_{s_p}}{\rho_{ab}d\forall_{ab_p}c_{p_\mathrm{p}}}\right)}_{\text{Source term}}=\underbrace{\frac{\partial T_p}{\partial t}}_{\text{Transient term}}
\end{aligned}\right\}\quad(6.26)$$

$$\text{here, }\left(\frac{\dot{q}_{s\_p}}{\rho_{ab}d\forall_{ab\_p}c_{p\_\mathrm{p}}}\right)=\begin{cases}\underbrace{\left(\frac{\dot{q}_{gen\_p}}{\rho_{ab}c_{p\_\mathrm{p}}}\right)}_{\text{Volumetric heat generation case}}\\ \underbrace{\left(\frac{2nr_h\dot{q}_{nu\_p}}{\rho_{ab}c_{p\_\mathrm{p}}(1-\varepsilon).r_{ab}^2}\right)}_{\text{Non-uniform heat flux case}}\end{cases}$$

$$\Rightarrow u_2\frac{\partial^2 T_p}{\partial z^2}+v_2(T_{cas}^4-T_p^4)+w_2(T_c^4-T_p^4)-x_2(\mathrm{T}_p-T_{a\_p})-y_2(\mathrm{T}_p-T_{rp})+z_2=\frac{\partial T_p}{\partial t}\quad(6.27)$$

Initial condition:

at $t=0, T_p=T_{atm}$

Boundary conditions are as follows:

At $z=0$,

$$\overbrace{k_p\frac{\partial T_p}{\partial z}=\sigma\in_{ab}(T_p^4-T_{atm}^4)+h_n(T_p-T_{atm})}^{\text{Volumetric heat generation}}\qquad\overbrace{-k_p\frac{\partial T_p}{\partial z}=q''_{in\_p}-\sigma\in_{ab}(T_p^4-T_{atm}^4)-h_n(T_p-T_{atm})}^{\text{Non-uniform heat flux}}$$

$$\underbrace{\qquad\qquad}_{\text{radiation}}\quad\underbrace{\qquad\qquad}_{\text{natural convection}}\qquad\underbrace{\qquad\qquad}_{\text{radiation}}\quad\underbrace{\qquad\qquad}_{\text{natural convection}}$$

Adiabatic boundary at $z = L$ $\dfrac{\partial T_p}{\partial z} = 0$.

Here, the heat loss due to natural convection is included and the required heat transfer coefficient is given by [Sharma *et al.*, (2015b)]:

$$h_n = \frac{NuK}{D} \text{ with } Nu = \left[0.60 + \frac{0.378 Ra_D^{1/6}}{\left\{1 + (0.559/\text{Pr})^{9/16}\right\}^{8/27}} \right]^2 . \qquad (6.27a)$$

Where,

$\dot{q}_{in\_p} = (POA)_p / A_{p\_c}$,

$A_{p\_c} = (1-\varepsilon)\pi r_{ab}^2$,

$dA_{nh} = 2\pi n r_h dz$,

$dA_{p\_s} = 2\pi r_{ab} dz \times 1/6$,

$dA_{pl} = 2\pi r_{ab} dz \times 1/2$,

$dA_{pu} = L_{pu} dz$,

$d\forall_{ab\_p} = (1-\varepsilon)\pi r_{ab}^2 dz$,

$$u_2 = \left(\frac{k_p}{\rho_p c_{p\_p}} \right),$$

$$v_2 = \frac{\sigma}{\rho_{ab} c_{p\_p} \left[\left(\frac{1-\in_{ab}}{\in_{ab}} \right) \left(\frac{(1-\varepsilon)\pi r_{ab}^2}{L_{pu}} \right) + \frac{(1-\varepsilon)\pi r_{ab}^2}{L_{pu} F_{pu-cas}} + \left(\frac{1-\in_{cas}}{\in_{cas}} \right) \left(\frac{3(1-\varepsilon) r_{ab}^2}{r_{cas\_i}} \right) \right]},$$

$$w_2 = \frac{\sigma}{\rho_{ab} c_{p\_p} \left[\left(\frac{1-\in_{ab}}{\in_{ab}} \right) \left((1-\varepsilon) 3\pi r_{ab} \right) + \frac{(1-\varepsilon) 3\pi r_{ab}}{F_{c-pl}} + \left(\frac{1-\in_{ab}}{\in_{ab}} \right) (1-\varepsilon) r_{ab} \right]},$$

$$x_2 = \left(\frac{2n h_{a\_p} r_h}{\rho_p c_{p\_p} (1-\varepsilon) . r_{ab}^{\ 2}} \right),$$

$$y_2 = \left(\frac{2 h_{rp\_p}}{\rho_p c_{p\_p} (1-\varepsilon) . r_{ab}} \right),$$

$$z_2 = \left(\frac{\dot{q}_{s\_p}}{\rho_{ab} d\forall_{ab\_p} c_{p\_p}} \right).$$

6.2.2.2 Central Absorber

The central absorber is surrounded by peripheral absorbers. On-the-field conditions, it receives the highest irradiance due to the quasi-Gaussian distribution of heat flux. It exchanges heat with peripheral absorbers via radiation, and with primary/return air via convection. The analysis for uniform and non-uniform heat flux distribution (Figure 6.8) is as follows:

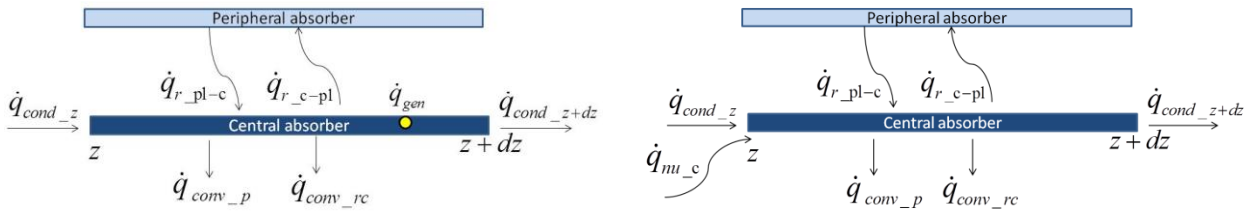

(a): Volumetric heat generation (b): Non-uniform heat flux

Figure 6.8: Energy balance for central absorber.

The energy balance for central absorber is:

Rate of energy in ($\dot{q}_{in}$) = Rate of heat conduction at z ($\dot{q}_{cond\_z}$) + Rate of radiative heat exchange from peripheral absorber ($\dot{q}_{r\_pl-c}$) + Rate of incident concentrated irradiance from heliostats ($\dot{q}_{nu\_c}$)

Rate of energy out ($\dot{q}_{out}$) = Rate of convective heat transfer to primary air ($\dot{q}_{conv\_a\_c}$) + Rate of convective heat transfer to return air ($\dot{q}_{conv\_rc}$) + Rate of heat conduction at z+dz ($\dot{q}_{cond\_z+dz}$) + Rate of radiation heat exchange from casing ($\dot{q}_{r\_c-pl}$)

Rate of internal heat generation in case of volumetric heating ($\dot{q}_{gen}$) = $\dot{q}_{gen\_c} d\forall_{ab\_c}$

Rate of energy stored ($\dot{q}_{st}$) = $\rho_{ab} d\forall_{ab\_c} c_{p\_c} \dfrac{\partial T_c}{\partial t}$

$\dot{q}_{in} - \dot{q}_{out} + \dot{q}_{gen} = \dot{q}_{st}$

The energy balance finally gives:

$$\left.\begin{aligned} &\underbrace{k_c A_{c\_c} \frac{\partial^2 T_c}{\partial z^2}.\mathrm{dz}}_{\textit{Conduction term}} - \underbrace{\frac{\sigma(T_c^4 - T_p^4)}{\rho_{ab} c_{p\_c} d\forall_{ab\_c}\left[\left(\frac{1-\in_{ab}}{\in_{ab} dA_{c\_s}}\right) + \frac{1}{dA_{c\_s} F_{c-pl}} + \left(\frac{1-\in_{ab}}{\in_{ab} dA_{pl}}\right)\right]}}_{\text{Net radiative het exchange at the central absorber}} - \underbrace{h_{a\_c} dA_{nh\_c}(\mathrm{T}_c - T_{a\_c})}_{\text{Convective loss to primary air}} \\ &\underbrace{-h_{rc\_c} dA_{c\_s}(\mathrm{T}_c - T_{rc})}_{\text{Convective loss to return air}} + \underbrace{\dot{q}_{s\_c}}_{\textit{Source}\text{ term}} = \underbrace{\rho_{ab} d\forall_{ab\_c} c_{p\_c} \frac{\partial T_c}{\partial t}}_{\text{Storage term}} \end{aligned}\right\} \quad (6.28)$$

$$\textit{here, } \dot{q}_{s\_c} = \begin{cases} \underbrace{\dot{q}_{gen\_c} d\forall_{ab\_c}}_{\textit{Volumetric}\text{ heat generation}} \\ \underbrace{q''_{nu\_c} dA_{nh\_c}}_{\textit{Non-uniform}\text{ heat flux}} \end{cases}$$

Simplification of eq. (6.28) gives the following equation:

$$\left.\begin{aligned} &\underbrace{\left(\frac{k_c}{\rho_{ab} c_{p\_c}}\right)\frac{\partial^2 T_c}{\partial z^2}}_{\textit{Conduction term}} - \underbrace{\left(\frac{2nh_{a\_c}\,\mathrm{r}_h}{\rho_{ab}(1-\varepsilon) r_{ab}^2 c_{p\_c}}\right)(\mathrm{T}_c - T_{a\_c})}_{\text{Convective loss to primary air}} \\ &\Rightarrow \underbrace{-\frac{\sigma(T_c^4 - T_p^4)}{\rho_{ab} c_{p\_c}\left[\left(\frac{1-\in_{ab}}{\in_{ab}}\right)\left(\frac{(1-\varepsilon) r_{ab}}{2}\right) + \frac{(1-\varepsilon) r_{ab}}{2F_{c-pl}} + \left(\frac{1-\in_{ab}}{\in_{ab}}\right)\left(\frac{(1-\varepsilon) r_{ab}}{6}\right)\right]}}_{\text{Radiative het exchange with peripheral absorber}} \\ &\underbrace{-\left(\frac{2h_{rc\_c}}{\rho_{ab}(1-\varepsilon) r_{ab} c_{p\_c}}\right)(\mathrm{T}_c - T_{rc})}_{\text{Convective loss to return air}} + \underbrace{\frac{\dot{q}_{s\_c}}{\rho_{ab} d\forall_{ab\_c} c_{p\_c}}}_{\textit{Source}\text{ term}} = \underbrace{\frac{\partial T_c}{\partial t}}_{\textit{Transient}\text{ term}} \end{aligned}\right\} \quad (6.29)$$

$$here,\ \left(\frac{\dot{q}_{s\_c}}{\rho_{ab} d\forall_{ab\_c} c_{p\_c}}\right) = \begin{cases} \underbrace{\left(\frac{\dot{q}_{gen\_c}}{\rho_{ab} c_{p\_c}}\right)}_{Volumetric\ \text{heat generation case}} \\ \underbrace{\left(\frac{2nr_h \dot{q}_{nu\_c}}{\rho_{ab} c_{p\_c}(1-\varepsilon).r_{ab}^2}\right)}_{Non-uniform\ \text{heat flux case}} \end{cases}$$

$$\Rightarrow u_3 \frac{\partial^2 T_c}{\partial z^2} - v_3(T_c - T_{a\_c}) - w_3(T_c^4 - T_p^4) - x_3(T_c - T_{rc}) + y_3 = \frac{\partial T_c}{\partial t} \qquad (6.30)$$

Initial condition:

At t = 0, $T_c = T_{atm}$

Boundary conditions:

At $z = 0$

$$\overbrace{k_c \frac{\partial T_c}{\partial z} = \sigma \in_{ab} (T_c^4 - T_{atm}^4) + h_n (T_c - T_{atm})}^{\text{Volumetric heat generation}} \quad \overbrace{-k_c \frac{\partial T_c}{\partial z} = q''_{in\_c} - \sigma \in_{ab} (T_c^4 - T_{atm}^4) - h_n (T_c - T_{atm})}^{\text{Non-uniform heat flux}}$$

radiation *natural convection* *radiation* *natural convection*

Adiabatic boundary at $z = L$, $\frac{\partial T_c}{\partial z} = 0$

The natural convection heat loss in central absorber is modeled using the correlation given in eq. (6.27a) as in the peripheral absorber.

Here,

$\dot{q}_{in\_c} = (POA)_c / A_{c\_c}$,

$A_{c\_c} = (1-\varepsilon)\pi r_{ab}^2 \times 1/6$,

$dA_{nh} = 2\pi n r_h dz \times 1/6$,

$dA_{c\_s} = 2\pi r_{ab} dz \times 1/6$,

$d\forall_{ab\_c} = (1-\varepsilon)\pi r_{ab}^2 .dz \times 1/6$,

$u_3 = \left(\frac{k_c}{\rho_{ab} c_{p\_c}}\right)$,

$v_3 = \left(\frac{2nh_{a\_c} r_h}{\rho_{ab}(1-\varepsilon) r_{ab}^2 c_{p\_c}}\right)$,

$$w_3 = \frac{\sigma}{\rho_{ab} c_{p\_c}\left[\left(\frac{1-\in_{ab}}{\in_{ab}}\right)\left(\frac{(1-\varepsilon)r_{ab}}{2}\right) + \frac{(1-\varepsilon)r_{ab}}{2F_{c-pl}} + \left(\frac{1-\in_{ab}}{\in_{ab}}\right)\left(\frac{(1-\varepsilon)r_{ab}}{6}\right)\right]},$$

$x_3 = \left(\frac{2h_{rc\_c}}{\rho_{ab}(1-\varepsilon) r_{ab} c_{p\_c}}\right)$,

$y_3 = \frac{\dot{q}_{s\_c}}{\rho_{ab} d\forall_{ab\_c} c_{p\_c}}$.

6.2.3 Primary Air

The convective heat transfer takes place during the interaction between primary air and absorbers, as shown in Figure 6.9. The equations for instantaneous energy balance in primary air are derived for both peripheral and central absorbers as:

Rate of energy in ($\dot{q}_{in}$) = Rate of energy transport at z + Rate of convective heat transfer from absorber to primary air ($\dot{q}_{conv\_a\_c/p}$) + Rate of heat conduction at z+dz ($\dot{q}_{cond\_z+dz}$)

Rate of energy out ($\dot{q}_{out}$) = Rate of energy transport at z+dz + Rate of heat conduction at z ($\dot{q}_{cond\_z}$)

Rate of internal heat generation ($\dot{q}_{gen}$) = 0

Rate of energy stored ($\dot{q}_{st}$) = $\rho_{a\_p} d\forall_{a\_p} c_{p\_ap} \frac{\partial T_{a\_p}}{\partial t}$ for primary air in peripheral absorber

Rate of energy stored ($\dot{q}_{st}$) = $\rho_{a\_c} d\forall_{a\_c} c_{p\_ac} \frac{\partial T_{a\_c}}{\partial t}$ for primary air in central absorber

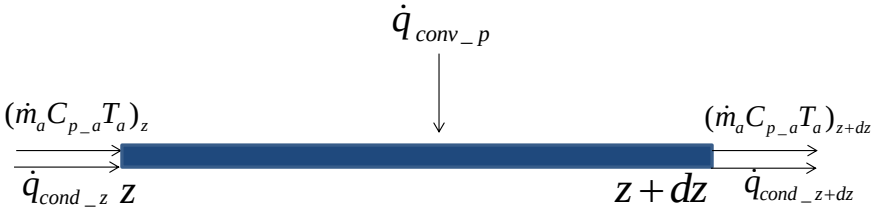

Figure 6.9: Energy balance in primary air.

$\dot{q}_{in} - \dot{q}_{out} + \dot{q}_{gen} = \dot{q}_{st}$

Energy balance gives:

6.2.3.1 Primary Air Flow in Peripheral Absorber

$$\underbrace{k_{pa} A_{a\_p} \frac{\partial^2 T_{a\_p}}{\partial z^2}.dz}_{\text{Conduction term}} \quad \underbrace{-\dot{m}_{a\_p} c_{p\_ap} \frac{\partial T_{a\_p}}{\partial z}.dz}_{\text{Rate of change of thermal energy across dz}} \quad + \underbrace{h_{a\_p} dA_{nh\_p} (T_p - T_{a\_p})}_{\textit{Convective} \text{ heat gain}} = \underbrace{\rho_{a\_p} d\forall_{a\_p} c_{p\_ap} \frac{\partial T_{a\_p}}{\partial t}}_{\text{Storage term}} \qquad (6.31)$$

Simplifying eq. (6.31) yields eq. (6.32) as following:

$$\Rightarrow \frac{\partial T_{a\_p}}{\partial t} = \left(\frac{k_{pa}}{\rho_{a\_p} c_{p\_ap}} \right) \frac{\partial^2 T_{a\_p}}{\partial z^2} - \left(\frac{\dot{m}_{a\_p}}{n\pi \rho_{a\_p} r_h^2} \right) \frac{\partial T_{a\_p}}{\partial z} + \left(\frac{2h_{a\_p}}{\rho_{a\_p} c_{p\_ap} r_h} \right) (T_p - T_{a\_p}) \qquad (6.32)$$

Initial condition:
At t = 0, $T_{a\_p} = T_{atm}$.

Boundary conditions:
At inlet (z = *0*), $T_{a\_p} = ARR \times T_{rp}\big|_{z=0} + (1 - ARR) T_{atm}$.

At the outlet (z = *L)* is given by, $\frac{\partial T_{a\_p}}{\partial z} = 0.$

6.2.3.2 Primary Air Flow in Central Absorber

$$\underbrace{k_{ca} A_{a\_c} \frac{\partial^2 T_{a\_c}}{\partial z^2}.dz}_{\text{Conduction term}} - \quad \underbrace{\dot{m}_{a\_c} c_{p\_ac} \frac{\partial T_{a\_c}}{\partial z}.dz}_{\text{Rate of change of thermal energy across dz}} \quad + \underbrace{h_{a\_c} dA_{nh\_c} (T_c - T_{a\_c})}_{\text{Convective heat gain term}} = \underbrace{\rho_{a\_c} d\forall_{a\_c} c_{p\_ac} \frac{\partial T_{a\_c}}{\partial t}}_{\text{Storage term}} \qquad (6.33)$$

Simplifying eq. (6.33) yields eq. (6.34) as following:

$$\Rightarrow \frac{\partial T_{a\_c}}{\partial t} = \left(\frac{k_{ca}}{\rho_{a\_c} c_{p\_ac}}\right)\frac{\partial^2 T_{a\_c}}{\partial z^2} - \left(\frac{6\dot{m}_{a\_c}}{n\pi\rho_{a\_c} r_h^2}\right)\frac{\partial T_{a\_c}}{\partial z} + \left(\frac{2h_{a\_c}}{\rho_{a\_c} c_{p\_ac} r_h}\right)(T_c - T_{a\_c}) \quad (6.34)$$

Initial condition:
At t = 0, $T_{a\_c} = T_{atm}$.
Boundary conditions:
The mixed air temperature at the inlet ($z = 0$) is given as, $T_{a\_c} = ARR \times T_{rc}\big|_{z=0} + (1 - ARR)T_{atm}$.
Adiabatic boundary condition at $z = L$ is given by, $\frac{\partial T_{a\_c}}{\partial z} = 0$.

Here,
$dA_{nh\_c} = 2\pi n r_h .dz \times 1/6,$
$dA_{nh\_p} = 2\pi n r_h dz,$
$d\forall_{a\_c} = n\pi r_h^2 dz \times 1/6,$
$d\forall_{a\_p} = n\pi r_h^2 dz.$

6.2.4 Return Air

The interaction of return air occurs with casing and absorbers (Figure 6.10). Heat balance equations are derived for return air in regions r_p and r_c respectively as:

Rate of energy in ($\dot{q}_{in}$) = Rate of energy transport at z+dz ($\dot{q}_{r\_z}$) + Rate of convective heat transfer from absorber($\dot{q}_{conv\_rc/rp\_c/p}$) + Rate of convective heat transfer from casing ($\dot{q}_{conv\_cas}$) + Rate of heat conduction at z ($\dot{q}_{cond\_z}$)

Rate of energy out ($\dot{q}_{out}$) = Rate of energy transport at z ($\dot{q}_{r\_z+\Delta z}$)+ Rate of heat conduction at z+dz ($\dot{q}_{cond\_z+dz}$)

Rate of internal heat generation ($\dot{q}_{gen}$) = 0

Rate of energy stored ($\dot{q}_{st}$) = $\rho_{rp} d\forall_{rp} c_{p\_rp} \frac{\partial T_{rp}}{\partial t}$ for region r_p

Rate of energy stored ($\dot{q}_{st}$) = $\rho_{rc} d\forall_{rc} c_{p\_rc} \frac{\partial T_{rc}}{\partial t}$ for region r_c

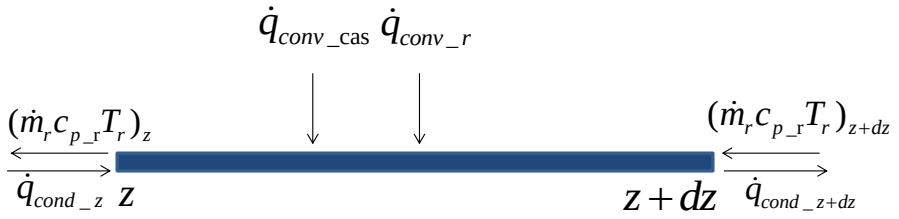

Figure 6.10: Energy balance in return air.

Energy balance gives

$\dot{q}_{in} - \dot{q}_{out} + \dot{q}_{gen} = \dot{q}_{st}$

6.2.4.1 Region r_p

$$\left.\begin{aligned} &\underbrace{k_{pr} A_{\mathrm{rp}} \frac{\partial^2 T_{rp}}{\partial \mathrm{z}^2}.\mathrm{dz}}_{\text{Conduction term}} + \underbrace{\dot{m}_{rp} c_{p\_\mathrm{rp}} \frac{\partial T_{rp}}{\partial \mathrm{z}}.\mathrm{dz}}_{\text{Rate of change of thermal energy across dz}} + \underbrace{h_{rp\_p} dA_{\mathrm{p\_s}} (\mathrm{T}_p - T_{rp})}_{\text{Convective heat exchange with peripheral absorber}} \\ &+ \underbrace{h_{rp\_cas} dA_{cas\_s} (\mathrm{T}_{cas} - T_{rp})}_{\text{Convective heat exchange with casing}} = \underbrace{\rho_{\mathrm{rp}} d\forall_{\mathrm{rp}} c_{p\_\mathrm{rp}} \frac{\partial T_{rp}}{\partial t}}_{\text{Storage term}} \end{aligned}\right\} \quad (6.35)$$

$$\begin{aligned} \frac{\partial T_{\mathrm{rp}}}{\partial t} &= \left(\frac{k_{pr}}{\rho_{rp} c_{p\_rp}}\right) \frac{\partial^2 T_{rp}}{\partial \mathrm{z}^2} + \left(\frac{\dot{m}_{rp}}{\rho_{rp} A_{rp}}\right) \frac{\partial T_{rp}}{\partial \mathrm{z}} + \left(\frac{\pi \mathrm{h}_{rp\_p} r_{ab}}{3\rho_{rp} c_{p\_rp} A_{rp}}\right) (\mathrm{T_p} - \mathrm{T}_{rp}) \\ &+ \left(\frac{\pi \mathrm{h}_{rp\_cas} r_{cas\_i}}{3\rho_{rp} c_{p\_rp} A_{rp}}\right) (\mathrm{T}_{cas\_i} - \mathrm{T}_{rp}) \end{aligned} \quad (6.36)$$

Initial condition:

At t = 0, $T_{rp} = T_{atm}$

Boundary conditions:

At the inlet of return air ($z = L$), $T_{rp} = T_{atm}$.

At the outlet of return air ($z = 0$), $\frac{\partial T_{rp}}{\partial \mathrm{z}} = 0.$

6.2.4.2 Region r_c

In region r_c, there is no interaction between return air and casing ($\dot{q}_{conv\_cas} = 0$).

$$\underbrace{k_{cr} A_{\mathrm{rc}} \frac{\partial^2 T_{rc}}{\partial \mathrm{z}^2}.\mathrm{dz}}_{\text{Conduction term}} + \underbrace{\dot{m}_{rc} c_{p\_\mathrm{rc}} \frac{\partial T_{rc}}{\partial \mathrm{z}}.\mathrm{dz}}_{\text{Rate of change of thermal energy across dz}} + \underbrace{h_{rc} dA_{\mathrm{c\_s}} (\mathrm{T}_c - T_{rc})}_{\text{Convective heat exchange with central absorber}} = \underbrace{\rho_{rc} d\forall_{rc} c_{p\_\mathrm{rc}} \frac{\partial T_{rc}}{\partial t}}_{\text{Storage term}} \quad (6.37)$$

$$\frac{\partial T_{\mathrm{rc}}}{\partial t} = \left(\frac{k_{cr}}{\rho_{rc} c_{p\_rc}}\right) \frac{\partial^2 T_{rc}}{\partial \mathrm{z}^2} + \left(\frac{6\dot{m}_{rc}}{\pi\rho_{rc} G(2r_{ab} + G)}\right) \frac{\partial T_{rc}}{\partial \mathrm{z}} + \left(\frac{2\mathrm{h}_{rc} r_{ab}}{\rho_{rc} c_{p\_rc} G(2r_{ab} + G)}\right) (\mathrm{T_c} - \mathrm{T}_{rc}) \quad (6.38)$$

Initial condition:

At t = 0, $T_{rc} = T_{atm}$.

Boundary conditions:

At the inlet ($z = L$), $T_{rc} = T_{atm}$.

At the outlet *($z = 0$)* i.e. $\frac{\partial T_{rc}}{\partial \mathrm{z}} = 0.$

where,

$A_{return} = \frac{\pi}{6}[r_{cas\_i}^2 - 7r_{ab}^2],$

$$A_{rc} = \frac{\pi}{6} \mathrm{G}[2r_{ab} + G],$$
$$A_{rp} = A_{return} - A_{rc},$$
$$d\forall_{rc} = A_{rc}.dz \times 1/6,$$
$$d\forall_{rp} = A_{rp} dz.$$

6.3 NUMERICAL SOLUTION

For the numerical solution, a fully implicit scheme which is first order in time and second order in space is developed. For solid domain, the radiation source term is linearized and the matrix formulation of the derived equations is as follows:

$$-\left[A_s\right]\left[T_{i+1}^{n+1}\right]_s^T + \left[B_s\right]\left[T_i^{n+1}\right]_s^T - \left[A_s\right]\left[T_{i-1}^{n+1}\right]_s^T = \left[T_i^n\right]_s^T + \left[C_s\right] \tag{6.39}$$

where, $[T]_s$ is the matrix containing temperature of the solid domain, $[A]_s$, $[B]_s$, $[C]_s$ and $[Z]_s$ are the coefficient matrices represented as follows:

$$\begin{aligned} \left[T\right]_s &= \left[T_{cas} \;\; T_p \;\; T_c\right] \\ \left[A\right]_s &= \left[A_1 \;\; A_2 \;\; A_3\right] \\ \left[B\right]_s &= \left[B_1 \;\; B_2 \;\; B_3\right] \\ \left[C\right]_s &= \left[C_1 \;\; C_2 \;\; C_3\right] \end{aligned} \tag{6.40}$$

The coefficients are as follows:

$$A_1 = \frac{U_1 \Delta t}{\Delta z^2},\; B_1 = 1 + \frac{2U_1 \Delta t}{\Delta z^2} + V_1 \Delta t,\; C_1 = W_1 \Delta t$$

here,

$\mathrm{U_1}=\mathrm{u_1}$, $\mathrm{V_1}=\mathrm{w_1}+4\mathrm{x_1}\mathrm{T}_{cas}^{*3}$, $\mathrm{W_2}=\mathrm{v_1}\dot{\mathrm{q}}_{CI}+\mathrm{w_1}\mathrm{T}_{rp}+\mathrm{x_1}\mathrm{T}_p^4+3\mathrm{x_1}\mathrm{T}_{cas}^{*4}$

$$A_2 = \frac{U_2 \Delta t}{\Delta z^2},\; B_2 = 1 + \frac{2U_2 \Delta t}{\Delta z^2} + V_2 \Delta t,\; C_2 = W_2 \Delta t$$

here,

$\mathrm{U_2}=\mathrm{u_2}$, $\mathrm{V_2}=4(\mathrm{v_2}+\mathrm{w_2})\mathrm{T}_p^{*3}$, $\mathrm{W_2}=3(\mathrm{v_2}+\mathrm{w_2})\mathrm{T}_p^{*4}-(\mathrm{u_2}+\mathrm{v_2})\mathrm{T}_p+\mathrm{v_2}\mathrm{T}_{cas}^4+\mathrm{w_2}\mathrm{T}_c^4 + x_2 T_{a\_p} + y_2 T_{rp} + z_2$

$$A_3 = \frac{U_3 \Delta t}{\Delta z^2},\; B_3 = 1 + \frac{2U_3 \Delta t}{\Delta z^2} + V_3 \Delta t,\; C_3 = W_3 \Delta t$$

here,

$\mathrm{U_3}=\mathrm{u_3}$, $\mathrm{V_3}=\mathrm{v_3}+4\mathrm{w_3}\mathrm{T}_c^{*3}+\mathrm{x_3}$, $\mathrm{W_2}=\mathrm{v_3}T_{a\_c} + 3w_3 T_c^{*4} - w_3 T_p^4 + x_3 T_{rc} + y_3$

For the fluid domain the set of linear equations in matrix formulation are as follows:

$$\left[A_f\right]\left[T_{i+1}^{n+1}\right]_f^T - \left[B_f\right]\left[T_i^{n+1}\right]_f^T + \left[C_f\right]\left[T_{i-1}^{n+1}\right]_f^T = -\left[T_i^n\right]_f^T - \left[Z_f\right].\Delta t$$

where, $[T]_f$ is the matrix containing temperature of the fluid domain, $[A]_f$, $[B]_f$, $[C]_f$ and $[Z]_f$ are the coefficient matrices represented as follows:

$$\left[T\right]_f = \left[T_{a\_p} \;\; T_{a\_c} \;\; T_{rp} \;\; T_{rc}\right],$$

$$
\begin{aligned}
[A]_f &= [A_4 \;\; A_5 \;\; A_6 \;\; A_7], \\
[B]_f &= [B_4 \;\; B_5 \;\; B_6 \;\; B_7], \\
[C]_f &= [C_4 \;\; C_5 \;\; C_6 \;\; C_7], \\
[Z]_f &= [Z_4 \;\; Z_5 \;\; Z_6 \;\; Z_7].
\end{aligned} \tag{6.41}
$$

Where,

$$A_4 = \frac{K_{pa}\Delta t}{\rho_{a\_p} c_{p\_ap} \Delta z^2} - \frac{\dot{m}_{a\_p}\Delta t}{2n\pi\rho_{a\_p} r_h^2 \Delta z},\; B_4 = \frac{2K_{pa}\Delta t}{\rho_{a\_p} c_{p\_ap} \Delta z^2} + \frac{2h_{a\_p}\Delta t}{\rho_{a\_p} c_{p\_ap} r_h} + 1,$$

$$C_4 = \frac{K_{pa}\Delta t}{\rho_{a\_p} c_{p\_ap} \Delta z^2} + \frac{\dot{m}_{a\_p}\Delta t}{2n\pi\rho_{a\_p} r_h^2 \Delta z},\; Z_4 = \frac{2h_{a\_p} T_p}{\rho_{a\_p} c_{p\_ap} r_h}$$

$$A_5 = \frac{K_{ca}\Delta t}{\rho_{a\_c} c_{p\_ac} \Delta z^2} - \frac{\dot{m}_{a\_c}\Delta t}{2n\pi\rho_{a\_c} r_h^2 \Delta z},\; B_5 = \frac{2K_{ca}\Delta t}{\rho_{a\_c} c_{p\_ac} \Delta z^2} + \frac{2h_{a\_c}\Delta t}{\rho_{a\_c} c_{p\_ac} r_h} + 1,$$

$$C_5 = \frac{K_{ca}\Delta t}{\rho_{a\_c} c_{p\_ac} \Delta z^2} + \frac{\dot{m}_{a\_c}\Delta t}{2n\pi\rho_{a\_c} r_h^2 \Delta z},\; Z_5 = \frac{2h_{a\_c} T_c}{\rho_{a\_c} c_{p\_ac} r_h}$$

$$A_6 = \frac{K_{pr}\Delta t}{\rho_{rp} c_{p\_rp} \Delta z^2} + \frac{\dot{m}_{rp}\Delta t}{2\rho_{rp} A_{rp} \Delta z},\; B_6 = \frac{2K_{pr}\Delta t}{\rho_{rp} c_{p\_rp} \Delta z^2} + \left(\frac{\pi h_{rp\_p} r_{ab}\Delta t + \pi h_{rp\_cas} r_{cas\_i}\Delta t}{3\rho_{rp} c_{p\_rp} A_{rp}} \right) + 1,$$

$$C_6 = \frac{K_{pr}\Delta t}{\rho_{rp} c_{p\_rp} \Delta z^2} - \frac{\dot{m}_{rp}\Delta t}{2\rho_{rp} A_{rp} \Delta z},\; Z_6 = \left(\frac{\pi h_{rp\_p} r_{ab} T_p + \pi h_{rp\_cas} r_{cas\_i}}{3\rho_{rp} c_{p\_rp} A_{rp}} \right)$$

$$A_7 = \frac{K_{cr}\Delta t}{\rho_{rc} c_{p\_rc} \Delta z^2} + \frac{6\dot{m}_{rc}\Delta t}{2\pi\rho_{rc} G(2r_{ab} + G)\Delta z},\; B_7 = \frac{2K_{cr}\Delta t}{\rho_{rc} c_{p\_rc} \Delta z^2} + \left(\frac{2h_{rc} r_{ab}\Delta t}{\rho_{rc} c_{p\_rc} G(2r_{ab} + G)} \right) + 1,$$

$$C_7 = \frac{K_{cr}\Delta t}{\rho_{rc} c_{p\_rc} \Delta z^2} - \frac{6\dot{m}_{rc}\Delta t}{2\pi\rho_{rc} G(2r_{ab} + G)\Delta z},\; Z_7 = \left(\frac{2h_{rc} r_{ab} T_c}{\rho_{rc} c_{p\_rc} G(2r_{ab} + G)} \right)$$

6.4 RESULTS AND DISCUSSION

6.4.1 Validation

A comparison of the measured and computed primary air temperature in a peripheral absorber is shown in Figure 6.11(a) at the steady state. The experiments were performed at an input power of 750 W and for a power to air mass flow rate ratio of about 140 kJ/kg. In these experiments Joule heating was applied on the circumference of absorber. That has resulted in volumetric type heating effect and was reported in Sharma *et al*., (2015a, b). The computed values using the different heat transfer coefficients (Table 6.1) are mostly within 5% of the measurements and is well within the reported uncertainty. A comparison between the computed and experiment based the thermal efficiency is presented in Figure 6.11(b). The values are collected from different literature and are indicated in this figure. The analyses using the correlation as in Kays *et al*., (1972) generally over-predict the thermal efficiency. The computed efficiency using Žukauskas, (1972) and Grimison, (1937) envelops the experimental data over a wide range of power to mass flow rate ratio with an acceptable variation. Finally, based on these investigations the derived correlation, especially, for the current receiver design by Sarma (2013) is selected for further analyses. As the next step, developed tool is validated using the measured time dependent air temperature at the outlet peripheral (T_{ap}) and central absorbers (T_{ac}). The reported experiment in Sharma *et al*., (2015b) at a flux concentration of

about 425 Suns, which corresponds to a power of 1500 W, and the power to air mass flow rate ratio of 300 kJ/kg is selected. A comparison between the computed and measured values of T_{ap} and T_{ac} up to about 2500 seconds is presented in Figure 6.11(c). The sharp rise in temperature within the first 300 seconds is well reproduced. This substantiates the applicability of the model during the unsteady phase. Moreover, the variation between the computed and measured values are well within the experiment uncertainty of about ± 7% as given in Sharma *et al.*, (2015b). Figure 6.11(d) compares the measured and computed outlet air temperature at the steady state at different values power to air mass flow ratio. Here, the input power is fixed at 750 W and the air mass flow rate is varied. The deviation between these values are well within ±7% and thus the applicability of the model is re-affirmed. It may be emphasized that the model is developed assuming straight pore based absorber. Thus, it may be concluded that the developed model will be helpful to scale-up a straight pore based receiver design in which the parameters are to be suitably adopted. The parametric investigations are presented subsequently to identify important parameters leading to an optimal absorber or a receiver design.

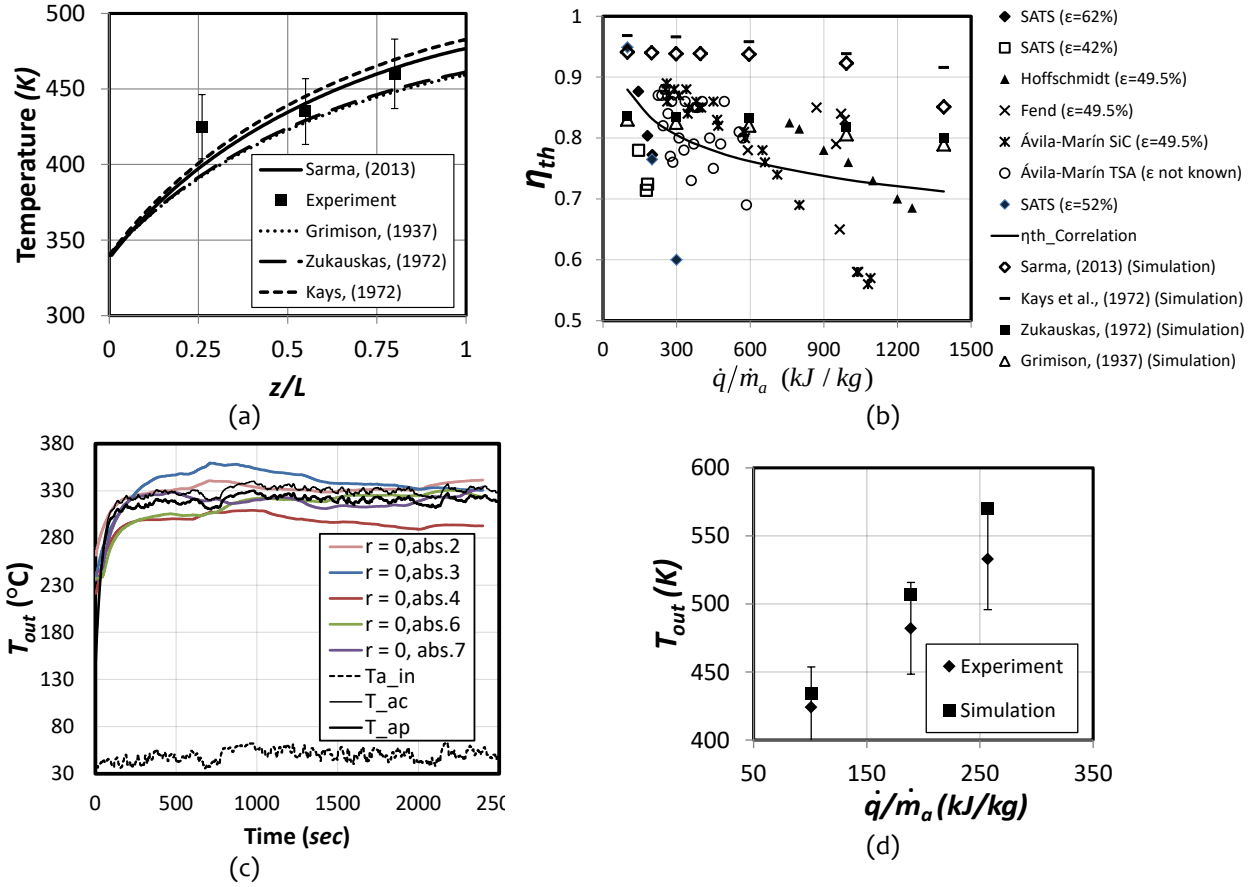

Figure 6.11: Comparison between the computed and measured (a) primary air temperature at the steady state and (b) thermal efficiencies, (c) time-dependent primary air temperature at the outlet of peripheral and central absorbers and (d) average primary air temperature at the absorber outlet at different power to air mass flow ratio.

6.4.2 Time Dependent Development of Temperature

It is observed that the steady state is achieved at around 500 seconds, see Figure 6.11(a). The time dependent temperature distribution in absorber material and in air along the flow direction is shown in Figure 6.12(a) and 6.12(b), respectively. This clearly demonstrates the initial sharp rise in temperature up to 100 seconds followed by a relatively slow change leading to the steady state. Consequently, the thermal stresses at the initiation is likely to be the highest in comparison to the steady state.

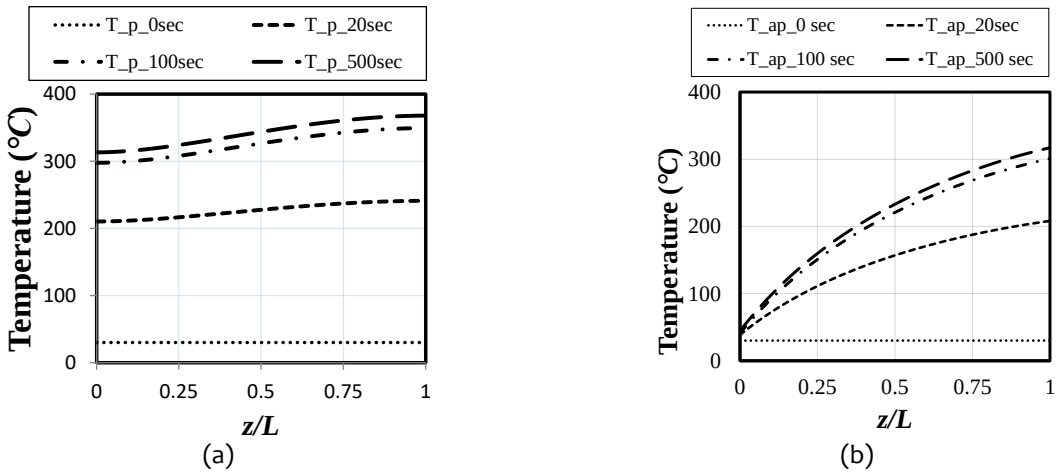

Figure 6.12: Time dependent development of temperature in (a) solid and (b) air.

6.4.3 Effect of Heat Flux Distribution

The central and peripheral absorbers are considered for analyzing the effect of heat flux distribution on the thermal efficiency and the temperature variation along the flow direction. The condition as in the reported experiment at a power of 1500 W and an air mass flow rate of about 5 g/s is used for this purpose. For this analysis the air return ratio is fixed at 0.6. The mass flow rate of return air around the central absorber is less than that of the peripheral absorber as a consequence of the offered higher flow resistance. Hence, the resulting Reynolds number for the return air will be lower around the central absorber in comparison to the peripheral absorber. This will lead to a reduction of heat transfer to the return air and consequently, an elevation in the temperature of central absorber. The same is clearly shown in Figure 6.13(a) and (b). The uniform heat flux distribution depicting volumetric heating results in a lower absorber temperature at the inlet surface (z/L = 0) in comparison to that of the outlet (z/L = 1). This substantiates that the volumetric heating effect is reproduced by the model as expected. On the other hand, the non-uniform heat flux distribution or non-volumetric heating leads to the highest absorber temperature at the inlet (see Figure 6.13(b)). Therefore, the heat loss via radiation and convection will be higher in case of the non-volumetric heating. As a consequence, a lower thermal efficiency is expected and hence, efforts are ongoing to improve design of absorbers to attain the volumetric heating as far as possible (see e.g. Luque *et al.*, 2018). An interesting observation is that the air temperature increases continuously from the inlet to outlet in case of volumetric heating while the same attains an asymptotic value in case of non-volumetric heating at $z/L \sim 0.75$. This means, the length of absorber may be reduced in case of non-volumetric heating leading to a lower parasitic loss, which is desirable. Thus, an optimal absorber design is expected.

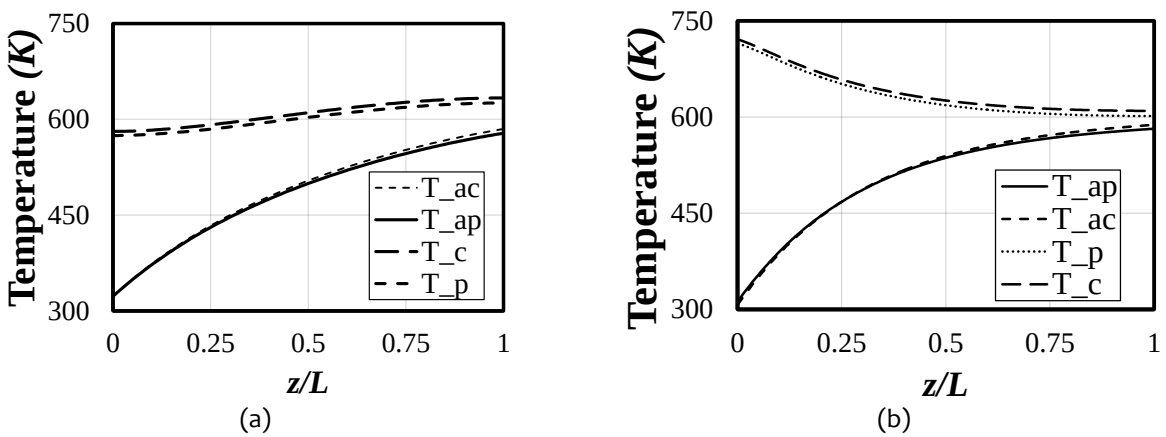

Figure 6.13: Axial variation of temperature in central (c) and peripheral absorbers (p) under (a) uniform and (b) non-uniform heat flux distribution; T_ap/T_ac: air; T_p/T_c: absorber. Air return ratio is 0.6.

6.4.4 Effect of Power to Air Mass Flow Rate Ratio

The computed values of thermal efficiency at the different power to air mass flow rate ratios ($\dot{q}/\dot{m}_a$) in the range of 100 – 1200 kJ/kg are shown in Figure 6.14. This is based on the straight pore based absorbers as discussed and the air return ratio is fixed at 0.6. This shows that the efficiency increases up to a power to air mass flow rate ratio of about 200 kJ/kg and subsequently decreases for the non-volumetric heating. Whereas, in case of volumetric heating the thermal efficiency remains, practically, comparable up to a power to air mass flow rate ratio of 600 kJ/kg. This is consistent with the provided details that the inlet surface temperature under these different conditions and the consequent loss to ambient. Interestingly, the outlet air temperature in case of volumetric heating is marginally higher than that of the non-volumetric heating. The analysis reveals that an optimal power to air mass flow ratio may be selected depending on the applications. Also, the gap between upper and lower limits indicates further possibilities of improvement in the existing designs.

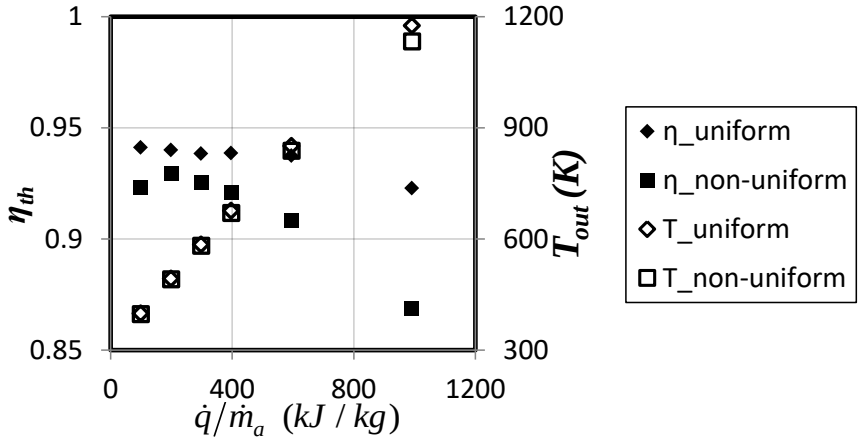

Figure 6.14: Variation of thermal efficiency with the ratio of power to air mass flow rate.

6.4.5 Effect of Absorber Porosity

The receiver thermal efficiency comprising of the straight pore based absorbers increases with porosity and attains an asymptotic value (see Figure 6.15). This may be attributed to the enhanced specific heat transfer surface to air from absorber and reduced flow resistance in case of a straight channel. Also, increasing the porosity will reduce the radiation and convection based heat loss from absorber surface to atmosphere as a result of the reduced exposed area. However, increasing porosity beyond say 80% may be detrimental as the material strength to withstand a high temperature and the thermal cycling will be affected. For a straight pore based absorber the maximum porosity of about 70 % is recommended as the efficiency reaches its practical limit, asymptotically, for the non-volumetric heating. In the case of volumetric heating the thermal efficiency may be limited to 90 %. The reason for a minor change in the slope of thermal efficiency at a porosity of about 80% is not obvious for the volumetric heating. Therefore, designing an absorber that promotes volumetric effect may allow exploiting the gap between these two values.

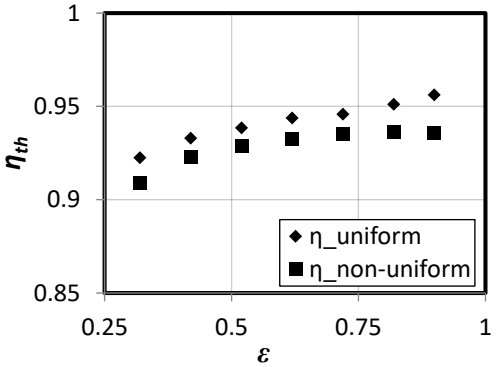

Figure 6.15: Variation of thermal efficiency with porosity of the absorbers.

6.4.6 Effect of Absorber Diameter

The computed thermal efficiency for the different values of absorber diameter to length ratio (d_{ab}/L) is presented in Figure 6.16. This shows an increasing trend for both the non-volumetric and volumetric heating up to $d_{ab}/L \sim 1$ for a straight pore based absorber design. For the non-volumetric heating a value of $d_{ab}/L \sim 0.8$ may be preferred in view of the reduced parasitic loss and noting the fact that air temperature reaches almost the maximum at a $d_{ab}/L \sim 0.8$ in Figure 6.13. The maximum absorber length may be limited to ~ 0.06 Re_d up to which the thermal boundary layer of air develops. The decrease in thermal efficiency beyond a $d_{ab}/L > 1.0$ may be attributed to the larger surface area of absorber, which is exposed to the return air. Thus, the convective heat loss from absorber surface to return air will increase and as a consequence the efficiency is likely to reduce. Thus, the developed model allows us selecting an optimal value of absorber diameter to length ratio. Interestingly, the selected value of absorber diameter to length of about 1.0 by Sharma *et al*. (2015a, 2015b) is substantiated by the presented analysis.

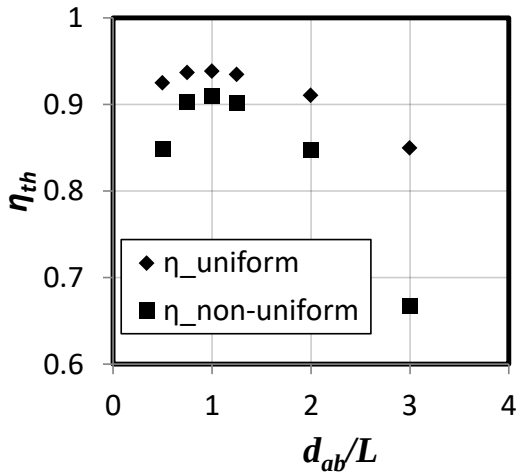

Figure 6.16: Variation of thermal efficiency with the absorber diameter to length ratio.

6.4.7 Effect of the Smallest Gap between Absorbers

A comparative assessment of the thermal efficiency with the ratio of smallest gap between absorbers to their length is shown in Figure 6.17. The zonal model is based on an assumption that the mass flux is constant throughout the cross section of return airflow region. Increasing the gap will lead to lesser fluid in contact with the absorber surface and reduced flow resistance. Furthermore, for a given mass flow rate of air ($\dot{m}_a$), the Reynolds number based on hydraulic diameter ($Re = 4\dot{m}_a/\pi D_h \mu$) will decrease with the gap between absorbers. All these will reduce the convective heat transfer to air from absorber surface resulting in increase in thermal efficiency of receiver. However, this will reduce the packing fraction of the absorber in a receiver or increase the void region at the receiver aperture, which is undesirable. Therefore, the smallest gap between two absorbers may be limited to 20% of the absorber length. In the reported experimental receiver, the smallest gap was ~5 mm or ~20% of the absorber length, which seems to be reasonable. Hence, the developed model provided us the limit to both the design parameters and operating condition that will lead to an optimal absorber and eventually the receiver design.

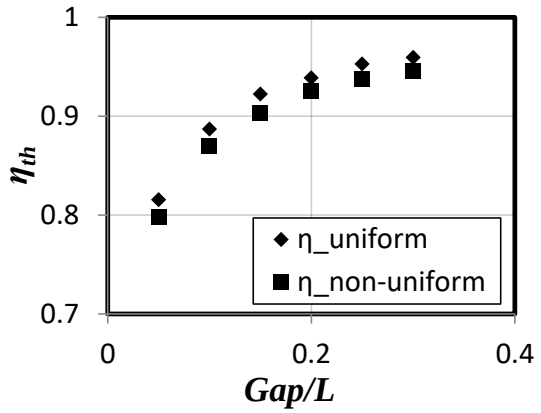

Figure 6.17: Variation of thermal efficiency with the smallest gap to absorber length ratio.

6.4.8 Effect of Air Return Ratio

As discussed earlier, the return air allows redistribution of absorber surface temperature, which is favorable. During this process a fraction of the input power is transferred to the return air and thus its recovery, as far as possible, is desired. The return air mixed with ambient increases its temperature at the absorber inlet depending on the extent of air return ratio. As a consequence, the heat transfer rate at the inlet may be affected due to a reduced temperature difference between absorber and the primary air. At the same time the outlet temperature of the air may increase for a given power input for a given thermal efficiency. Thus, the air temperature difference between the inlet and outlet of receiver remains practically unchanged. The same is illustrated in Figure 6.18 wherein the variation in thermal efficiency is negligible. However, as expected, the outlet temperature of air at the receiver outlet increases with increase in air return ratio. Hence, this corresponds to the waste heat recovery from the convective loss due to return air. Because a high outlet temperature at a given power to mass flow rate ratio is beneficial for the system, a receiver design with a high air return ratio is recommended for operation. Constraints regarding the use of suction may limit the value, however, efforts may be made to achieve at the least 0.7 air return ratio.

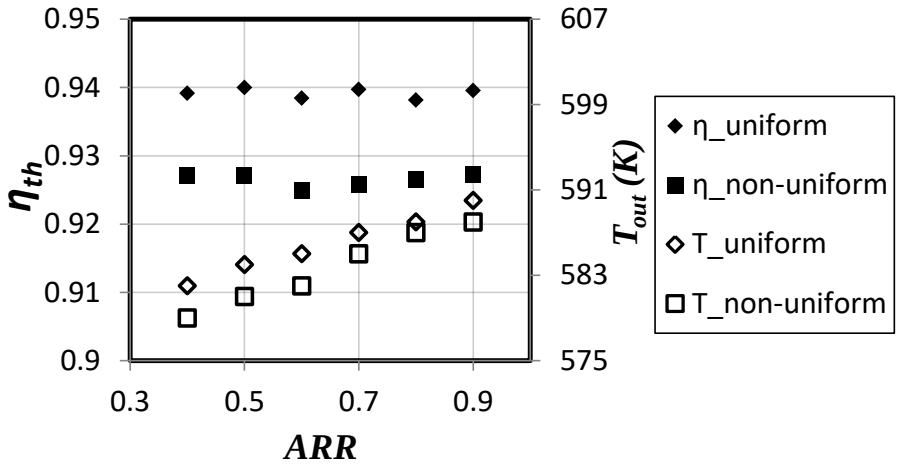

Figure 6.18: Variation of thermal efficiency and outlet air temperature with air return ratio (ARR).

6.4.9 Effect of differential heating

On-the-field conditions lends to a higher concentrated irradiance onto the central absorber due to the quasi-Gaussian distribution as shown in Figure 6.1. The effect of non-uniform heat flux on the heat transfer is simulated with the differential heating of absorbers. Here, the central absorber is subject to a higher heat flux in comparison to its peripheral counterparts. As in an experiment, the total input power to the receiver is 1500 W at an air mass flow rate of 5 g/s. Here, $q''_{central}/q''_{peripheral}$ denotes the ratio of input heat flux to the central and peripheral absorber. A minor decrease in the thermal efficiency for both the volumetric (uniform) and non-uniform absorber heating is observed with the increasing $q''_{central}/q''_{peripheral}$

(see Figure 6.19(a)). Figure 6.19(b) and (c) show the variation of solid and air temperature along the flow direction at $q''_{central}/q''_{peripheral}$ = 4. A much higher central absorber temperature in comparison to the the peripheral counterpart is observed. It may be noted that the temperature difference between peripheral and central absorbers are substantial in such an extreme condition. In fact, such observations necessitate the homogenization of heat flux distribution onto the absorber surface and the efforts are ongoing to achieve the same.

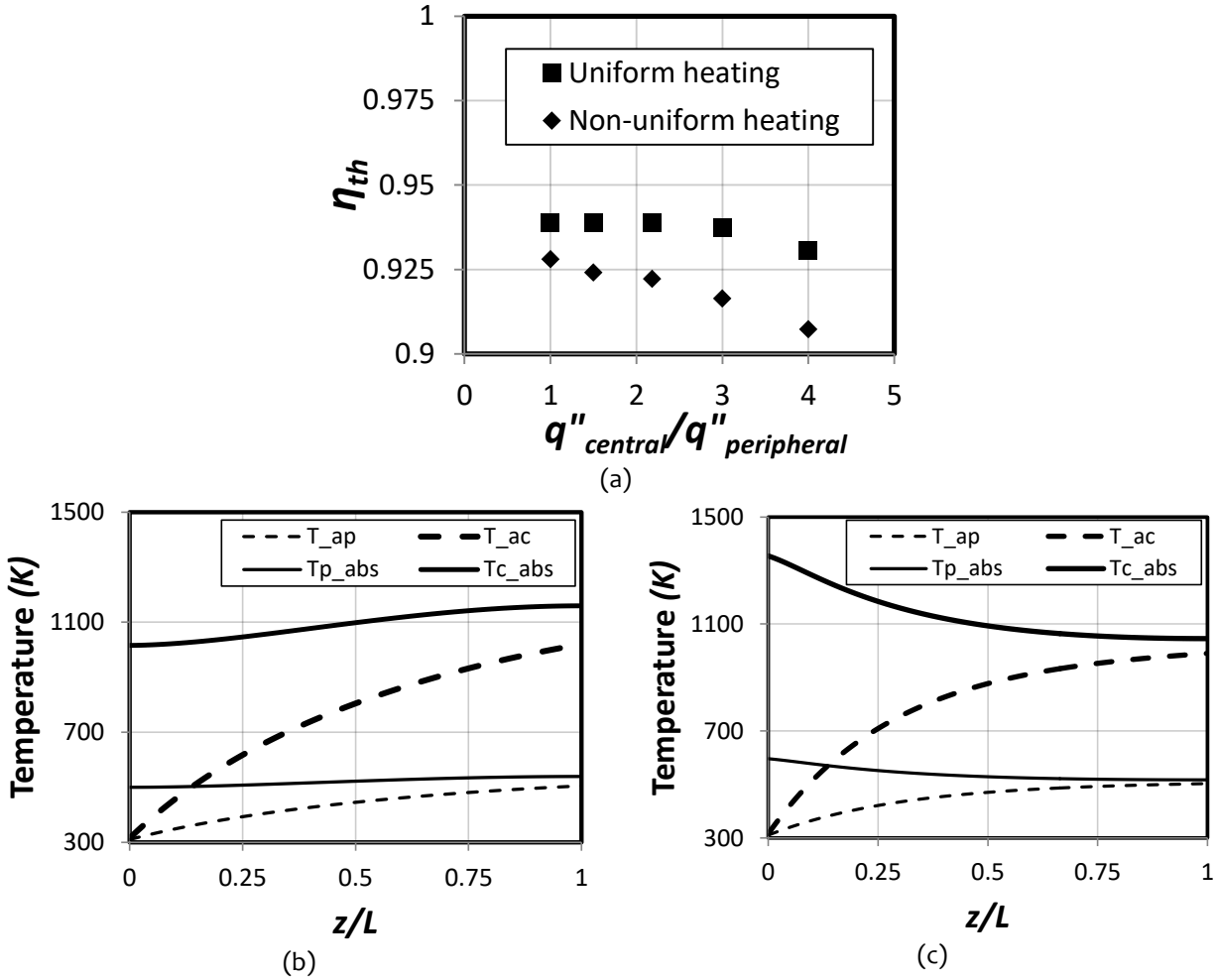

Figure 6.19: (a) Variation of thermal efficiency with differential heating ; Solid and air temperature along the flow direction ($q''_{central}/q''_{peripheral}$ = 4) under(b) volumetric heating and (c) non-uniform heat flux.

6.5 SUMMARY

The unsteady heat transfer analysis with the circular straight pores based open volumetric air receiver is performed in this chapter. A one-dimensional zonal model is developed for the same in which the absorbers are classified as central and peripheral followed by validation using the in-house and the reported experimental data. The analysis revealed the effect of various geometric and operational parameters on the performance of the receiver. The important conclusions and remarks are stated as follows:

a. The effect of heat flux distribution on the porous absorbers revealed that its non-uniformity lends to a higher absorber surface temperature at the inlet as compared to the volumetric heat generation. Therefore, the performance of the receiver is on the higher side in case of volumetric heating on the account of a low radiation and convection based heat losses. Operating the receiver at high power to air mass flow rate ratio (> 400 kJ/kg) is likely to decrease the thermal efficiency of the receiver.

b. Increment in the absorber porosity is beneficial in terms of the receiver performance. However, this must be restricted to an optimum value keeping the durability of the receiver in mind.

c. The analysis affirms that the absorber diameter must be selected based on the thermal entry length and the convective heat losses to return air. The current design of the absorber with $d_{ab}/L \sim 1$ is found as the most suitable choice in terms of the receiver performance.

d. The gap between the adjacent absorbers must be carefully selected. It is found that the thermal efficiency increase with increment in the shortest gap between the absorbers but at the same time, there will be an increase in void region at the front cross-section of the receiver. Such condition is not desirable as it reduces the incident concentrated solar irradiance in the actual conditions. Hence, the shortest gap between the absorbers must be selected as a balance between these factors.

e. The air return ratio affects the temperature of air at the outlet of the absorber. The outlet air temperature increases with increase in air return ratio, therefore, a receiver design with high air return ratio is recommended. However, a high air return ratio may increase the temperature of the front region of the receiver which may increase the absorber temperature. This may reduce the efficiency of the receiver and may even affect its durability.

Although, the radiative and convective heat losses are included besides the radiative heat exchange between the absorbers and casing but still there is a space for further improvements which may be added in future viz. the radiation based heat loss from the absorber pores, the effect of wind speed, the spectral dependence.

…